INVESTIGATION OF UV PHOTOIONIZATION SUSTAINED DISCHARGE FOR GAS LASERS

Richard C. Lund, et al

Hughes Research Laboratories

Prepared for:

Office of Naval Research
Advanced Research Project Agency

March 1974

UNCLASSIFIED

SECURITY CLASSIFICATION OF THIS PAGE (When Data Entered)

REPORT DOCUMENTATION PAGE		READ INSTRUCTIONS BEFORE COMPLETING FORM
1. REPORT NUMBER N00014-73-C-0287	2. GOVT ACCESSION NO.	3. RECIPIENT'S CATALOG NUMBER AD 775525
4. TITLE (and Subtitle) Investigation of UV Photoionization Sustained Discharge for Gas Lasers		5. TYPE OF REPORT & PERIOD COVERED Semiannual Tech. Rpt. 1 July 1973-31 Dec. 1973 6. PERFORMING ORG. REPORT NUMBER
7. AUTHOR(s) R.C. Lind, W.M. Clark, and J.Y. Wada		8. CONTRACT OR GRANT NUMBER(s) N00014-73-C-0287
9. PERFORMING ORGANIZATION NAME AND ADDRESS Hughes Research Laboratories 3011 Malibu Canyon Road Malibu, CA 90265		10. PROGRAM ELEMENT, PROJECT, TASK AREA & WORK UNIT NUMBERS Program Code No. 3E90 ARPA Order No. 1807
11. CONTROLLING OFFICE NAME AND ADDRESS Advanced Research Projects Agency 1400 Wilson Boulevard Arlington, VA 22209		12. REPORT DATE March 1974 13. NUMBER OF PAGES 53
14. MONITORING AGENCY NAME & ADDRESS (if different from Controlling Office) Office of Naval Research Department of the Navy Arlington, VA 22217		15. SECURITY CLASS. (of this report) Unclassified 15a. DECLASSIFICATION/DOWNGRADING SCHEDULE

16. DISTRIBUTION STATEMENT (of this Report)

17. DISTRIBUTION STATEMENT (of the abstract entered in Block 20, if different from Report)

18. SUPPLEMENTARY NOTES

19. KEY WORDS (Continue on reverse side if necessary and identify by block number)

Laser, Discharge, UV Radiation, Photoionization

20. ABSTRACT (Continue on reverse side if necessary and identify by block number)

The objectives of this program are to investigate and improve ultraviolet (uv) photoionization plasma conditioning techniques, to perform the demonstration of a uv sustained electrical discharge atmospheric pressure CO_2 laser, and to establish scalability limits.

Initially, fundamental experiments employing small scale (1 x 2 x 15 cm^3) discharge volumes established that in excess of

DD FORM 1 JAN 73 1473 EDITION OF 1 NOV 65 IS OBSOLETE

UNCLASSIFIED

SECURITY CLASSIFICATION OF THIS PAGE (When Data Entered)

200 J/ℓ-atm could be input to 1 atm CO_2 laser mixture by the uv photoionization of an added low ionization potential organic molecule. These and additional experiments led to conjectures for mixture mean free paths for certain critical CO_2, N_2, He tri-n-propylamine mixture ratios on the order of 8 cm.

Power extraction and small signal gain measurements were undertaken during this reporting period using a device with a larger discharge volume (2.5 x 15 x 50 cm^3) and an improved uv source configuration. Output energies in excess of 45 J/ℓ-atm with pulse lengths to 37 μs have been achieved.

The limits of scalability of the uv sustained plasma conditioning technique are now being addressed. A large volume (20 x 20 x 100 cm^3) discharge device is currently being designed for this purpose. The construction and extensive testing of this device will be undertaken during the coming period.

TABLE OF CONTENTS

LIST OF ILLUSTRATIONS

ABSTRACT

The objectives of this program are to investigate and improve ultraviolet (uv) photoionization plasma conditioning techniques, to perform the demonstration of a uv sustained electrical discharge atmospheric pressure CO_2 laser, and to establish scalability limits.

Initially, fundamental experiments employing small scale ($1 \times 2 \times 15$ cm^3) discharge volumes established that in excess of 200 J/ℓ-atm could be input to 1 atm CO_2 laser mixture by the uv photoionization of an added low ionization potential organic molecule. These and additional experiments led to conjectures for mixture mean free paths for certain critical CO_2, N_2, He tri-n-propylamine mixture ratios on the order of 8 cm.

Power extraction and small signal gain measurements were undertaken during this reporting period using a device with a larger discharge volume ($2.5 \times 15 \times 50$ cm^3) and an improved uv source configuration. Output energies in excess of 45 J/ℓ-atm with pulse lengths to 37 μs have been achieved.

The limits of scalability of the uv sustained plasma conditioning technique are now being addressed. A large volume ($20 \times 20 \times 100$ cm^3) discharge device is currently being designed for this purpose. The construction and extensive testing of this device will be undertaken during the coming period.

I. INTRODUCTION

The objective of this program is to investigate and improve ultraviolet (uv) photoionization plasma conditioning techniques. Within the scope of this objective is the specific goal of the demonstration of a uv sustained electrical discharge atmospheric pressure CO_2 laser. The dynamics of the plasma generation in this mode are similar to those of the electron beam controlled discharge; the voltage applied to the main discharge electrodes can be reduced below that required for a self-sustained avalanche mode. The principal advantage realized in this approach is complete control of the main discharge by the uv source at all times during operation.

The attractive feature of uv sustained as opposed to e-beam sustained operation is the simplicity of construction. Specifically, a foil is not required and the high voltages needed to give efficient electron penetration of the foil are not necessary.

The crucial questions that need to be answered through the research conducted during this program are (1) whether an electron density sufficient to sustain the discharge in a CO_2 laser mixture can be produced by a uv photoionization technique, specifically, plasma densities of 10^{12} electrons/cm^3 over pulse lengths of 20 μsec or longer must be attained, and (2) what the scalability parameters are for such a technique.

The first year program pursued to investigate these questions consisted basically of the following three tasks:

1. Determination of the emission spectrum and power saturation characteristics of uv spark sources operated in CO_2 laser mixture, metal vapors, and other gas additives

2. Development of seeding techniques which will improve the photoionization efficiency of the laser medium

3. Evaluation of uv photoionization sustained CO_2 laser gas discharge characteristics and laser performance via small signal gain and laser power output measurements.

During the first reporting period[1] results were obtained which eminated from the direction indicated by tasks one and two. The principal results (discussed in Section II) were: plasma densities required ($n_e \sim 10^{12}$ electrons/cm^3 for >20 μs) have been demonstrated, emission spectra of spark discharges have been obtained, and a mixture mean free path of 8 cm is conjectured for an appropriate mixture of CO_2, N_2, He and seed gas. Based on these results, baseline operating conditions for laser gas mixtures, seed gas concentrations, and uv intensities were established. These were then used as a guideline for laser measurements (Task 3) discussed in this report and for extensive scalability studies to be performed on the large scale device to be constructed during the follow-on program. The principal results obtained during this reporting period were the demonstration of up to 50 J/ℓ-atm laser output energy in a 37 μs (total) pulse length in a 2.5 x 15 x 50 cm^3 device in a completely uv sustained mode of operation and the design of a large volume 20 x 20 x 100 cm^3 discharge device for scalability studies.

II. SUMMARY OF PREVIOUS RESULTS

During the first reporting period, an extensive parametric investigation of the discharge input energy was undertaken in a small scale device which employed uv arc discharges located adjacent to the main discharge electrodes (see Fig. 1). Both the uv source and main discharge electrodes were mounted in a high vacuum glass enclosure to permit accurate control of the discharge environment. All internal supporting components were selected from those materials with low vapor pressure and outgassing properties and with high resistance to seed gas additives. Various mixture ratios of CO_2, N_2, He, seed gas concentrations, total pressures, and uv spark energies were studied to allow for a complete mapping of obtainable sustainer energy densities.

Before presenting the results of these experiments and in order to provide a theoretical basis for the assessment of these data, we will first discuss a calculation of the uv produced electron number density expected for such a system. In Fig. 2, the computed sustainer energy densities as a function of uv current are summarized for a wide range of gas mixtures. This calculation assumes single step photoionization of the added seed gas (in this example, tri-n-propylamine is used) and a recombination limited plasma. From this figure, we see two important effects. First, there is a minimum CO_2 concentration below which no further increase in sustainer energy results. As the CO_2 concentration decreases, the effective mixture mean free path is determined by the seed gas concentration. Second, there is a broad optimum in sustainer energy for a large (order of magnitude) change in seed gas concentration which produces only a small variation in the sustainer energy because at low seed gas concentrations the uv absorption characteristic is dictated by CO_2 molecules and only when the seed gas concentration is increased does the seed gas absorption play a dominant role. Both of these effects are critical to the determination of the limiting mean free path and hence the limit of scalability.

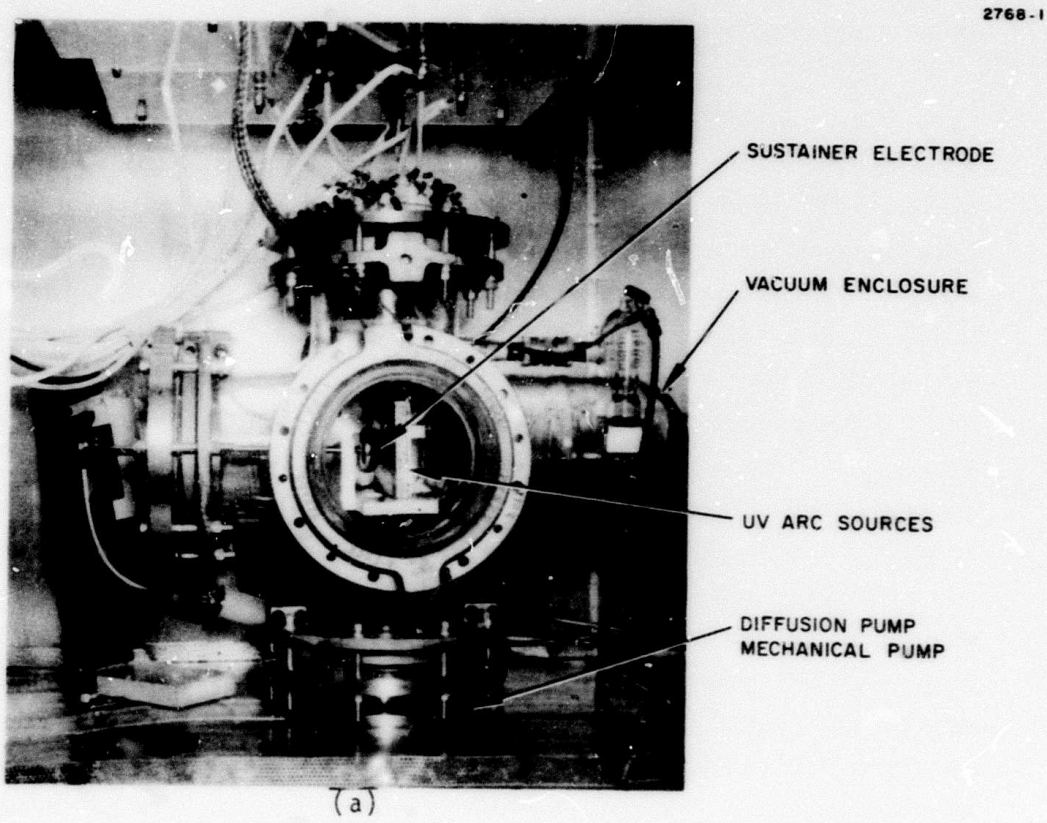

Fig. 1. Experimental uv sustained discharge device.

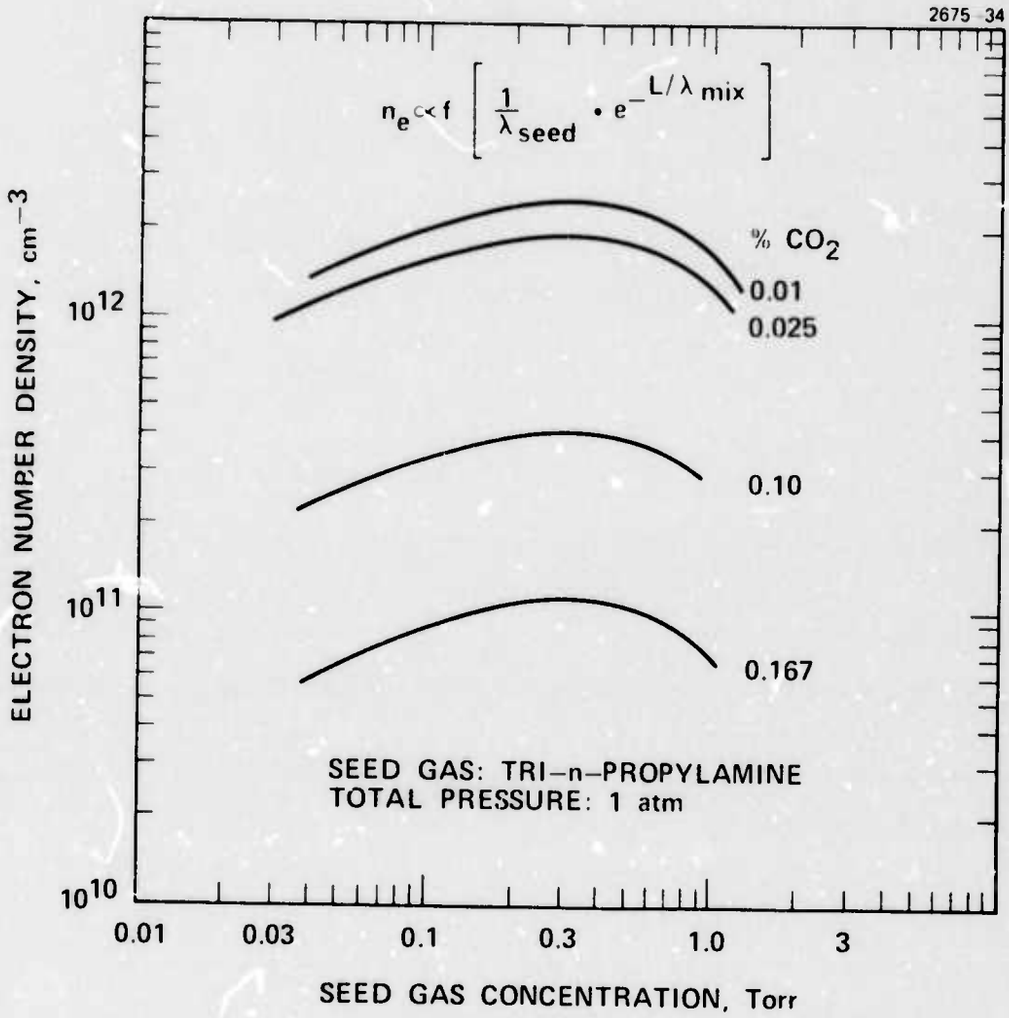

Fig. 2. Calculated electron number density.

Two of the results of the experimental study are shown in Figs. 3(a) and 3(b). First, in Fig. 3(a), the normalized sustainer energy obtained as a function of the normalized uv spark current is plotted for four mixture ratios and fixed seed gas concentrations while in Fig. 3(b), similar plots are for three seed gas concentrations with a fixed mixture ratio. We see that the results of these experiments do follow the trends predicted above.

Figure 4(a) gives a typical current waveform obtained and 4(b) gives the absolute sustainer energies obtained for the mixture producing the largest relative energy density results shown in the previous figures. With a uv spark current of 3 kA a value of 300 J/ℓ-atm has been obtained. The pulse lengths corresponding to these energies depend solely on the pulse length of the uv source; for the present case, this corresponds to an underdamped ringing arc circuit of approximately 50 μs in duration. Although 300 J/ℓ-atm is the input energy requirement for efficient CO_2 excitation, a considerable amount of uv energy is expended to achieve this level. Estimates of the uv energy based on the 3 kA spark current indicate that approximately equal amounts of energy are deposited in the uv sparks and the sustainer discharge. Further experimental measurements directed toward alleviating this undesirable situation have demonstrated that a substantial decrease in the amount of uv energy required can be obtained by the use of a type of "vacuum sliding spark" system (discussed in Section III).

The effective mean free paths of the CO_2 and seed gas molecules have been evaluated from such data and summarized in Table I. For a typical CO_2 mixture of 0.015 atm of CO_2 and 0.3 Torr of seed gas, the effective mean free paths are 11 cm and 20 cm, respectively, whereas the corresponding overall mixture mean free path is approximately 8 cm. As further conformation for this projected mean free path a characterization of the wavelengths responsible for the production of the observed photoionization of the added seed gases was undertaken. The results of such tests indicated that the observed dense plasma was produced by radiation with wavelengths

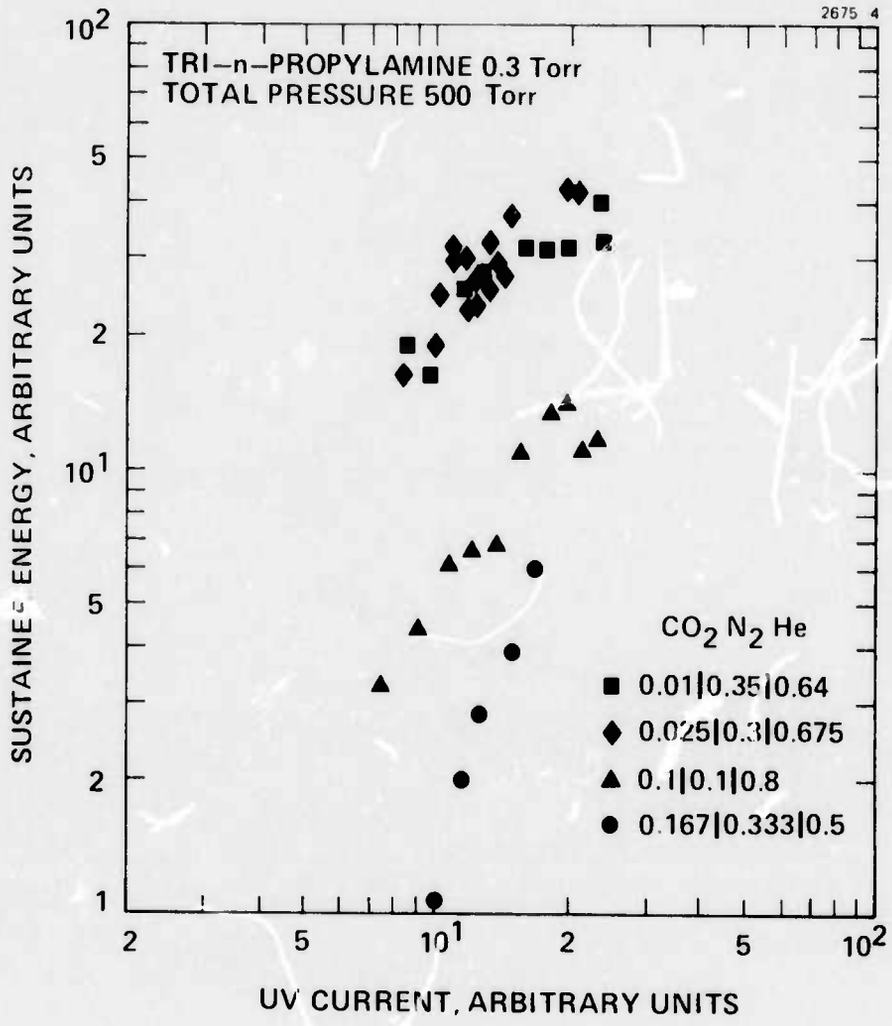

Fig. 3(a). Sustainer energy as a function of uv current for various laser mixtures.

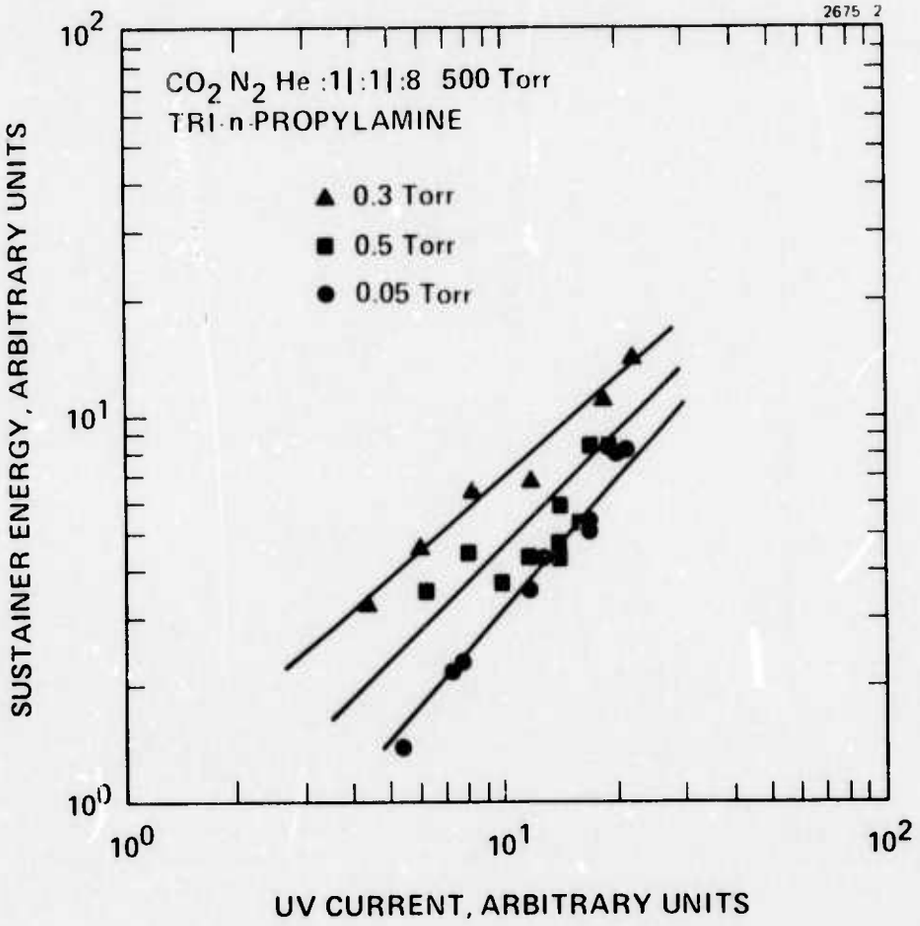

Fig. 3(b). Sustainer energy as a function of uv current for various concentrations of tri-n-propylamine.

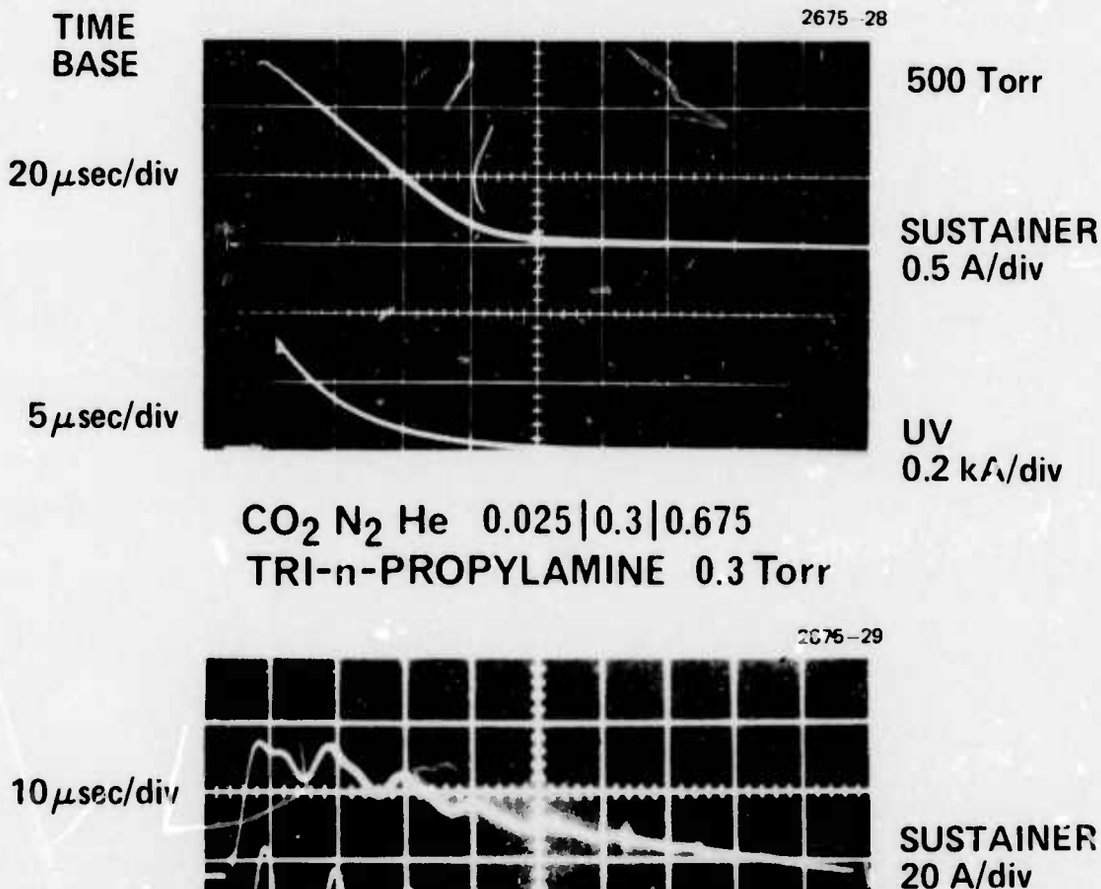

Fig. 4(a). Sustainer current and uv current waveforms.

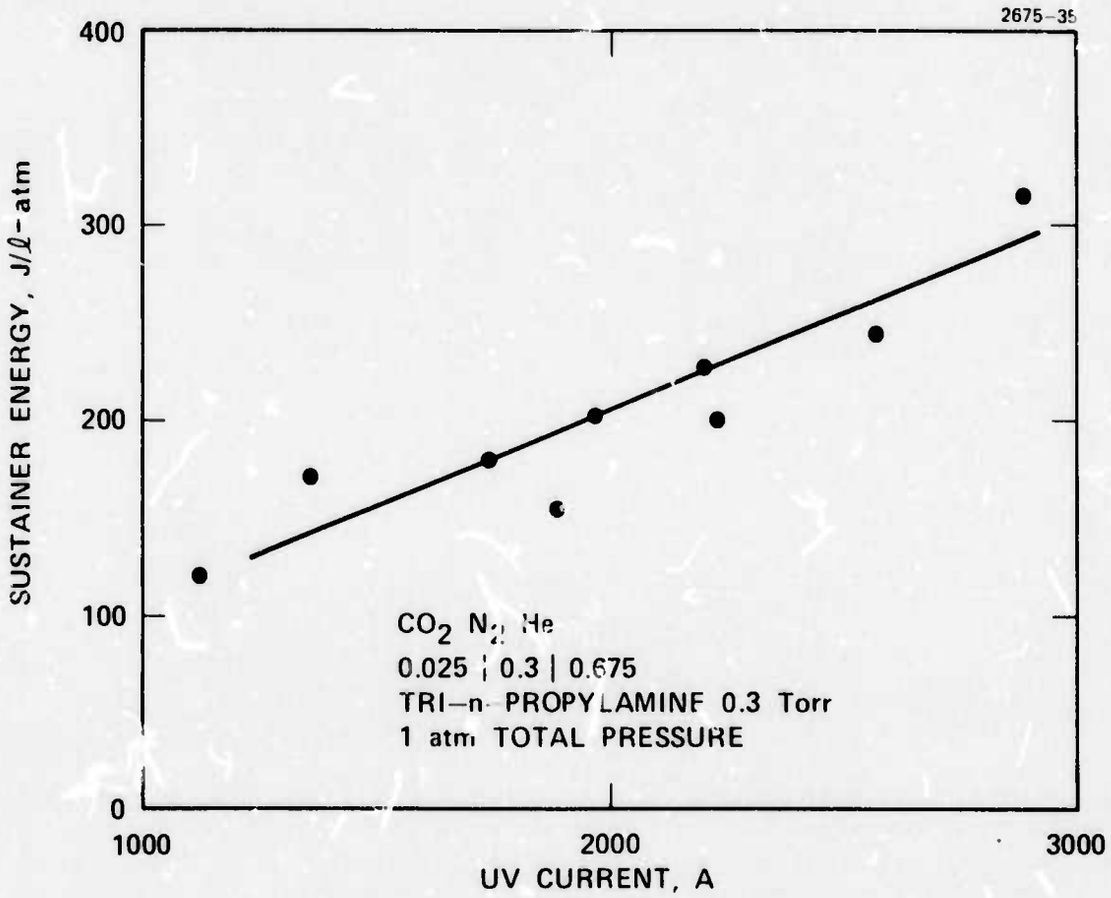

Fig. 4(b) Maximum input sustainer energy in J/ℓ-atm as a function of uv current in amps.

between approximately 1200 and 1700 Å with more than 60% between 1500 to 1700 Å. Such a result can be explained by examination of the mean free path through CO_2 shown in Fig. 5. Because the ionization potential of tri-n-propylamine is 1720 Å, we conclude that single step photoionization is the production mechanism for the plasma. It is clear from the mean free path shown that below 1200 Å no radiation is transmitted through any reasonable size device that uses CO_2; thus we arrive at the limiting wavelengths obtained experimentally.

TABLE I

Measured Effective Mean Free Paths of CO_2 and Seed (tri-n-propylamine) Gas

Molecules	Effective Mean Free Path[a] cm-Atm
CO_2	0.16
Tri-n-propylamine	8×10^{-3}

[a]Typical mixture of 1 atm: CO_2:N_2:He:seed gas 0.02:0.3:0.7:0.004.

T1195

Although these small-scaled experimental results provide optimized mixture ratios, they cannot discriminate whether these optimum mixtures are determined by the mean free path of the mixture becoming equal to or shorter than the device size or whether the available uv radiation could be used effectively if the device were larger. Such a consideration naturally leads to a study of larger scale devices. This study will be accomplished during the coming period (see Section IV) where a device of a size to test the conjectured 8 cm mean free path will be constructed and tested.

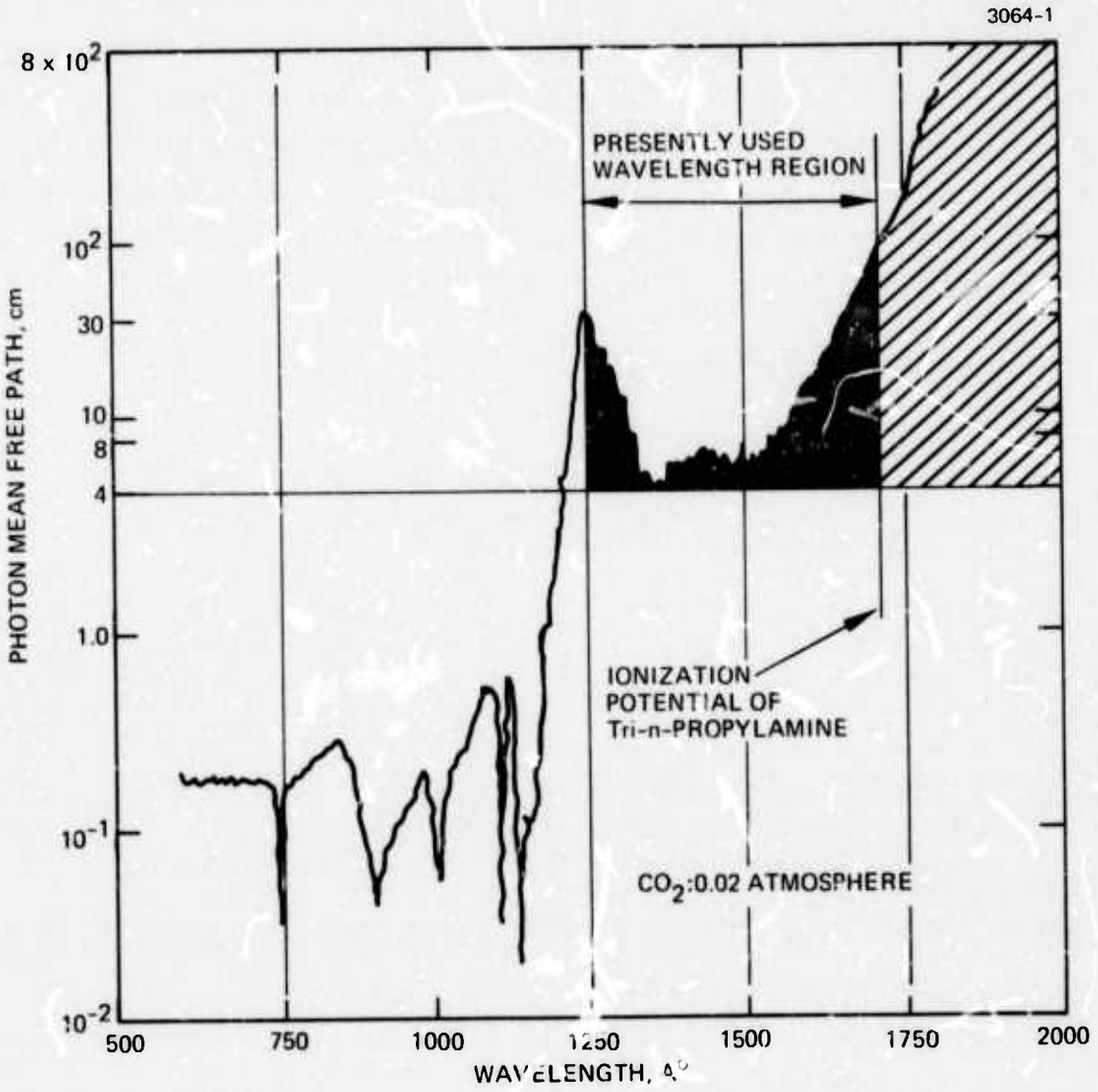

Fig. 5. UV photon mea. free path through CO_2 at 0.02 atm.

III. CO_2 LASER DEMONSTRATION AND UV SOURCE STUDIES

With the demonstration of the capability to obtain input discharge energy densities that will efficiently excite CO_2 laser mixtures, small signal gain distribution and power extraction measurements were then performed. To make such measurements, a larger discharge device was necessary because of expected low gain levels caused by the low CO_2 concentrations required. Consequently, a medium volume device ($2.5 \times 15 \times 50$ cm^3) using an improved uv source was employed and extensively tested. The results of such tests, along with discussions and calculations of uv energy and flux distribution requirements, are discussed in this section. The results to be presented play a significant role in the design of the large-scale device discussed in Section IV.

A. UV Energy Requirements

As discussed in Section II, attaining an input energy density in excess of 200 J/ℓ required a considerable amount of energy from the uv source. A more efficient source is needed to lower this requirement. One type of source that appears promising is the vacuum sliding spark (VSS).[2] The configuration (see Fig. 6) of the VSS studied to date is similar to that used by Richardson, et al.,[3] in their uv preionized laser studies. It consists of small copper squares located on an alumina dielectric surface with a low inductance copper ground plane below the alumina surface. Such a scheme produces a two-dimensional array of cascaded arc discharges across the dielectric substrate. Each row is energized by its own low inductance capacitor. The principal factor in the operation of this scheme is the small but finite capacitance to ground from each arc to the ground plane. This capacitance reduces the voltage drop required across the complete series of arcs to that required for self-breakdown of one only. Thus, the voltage remains at a high value and, therefore, the energy transfer is more efficient.

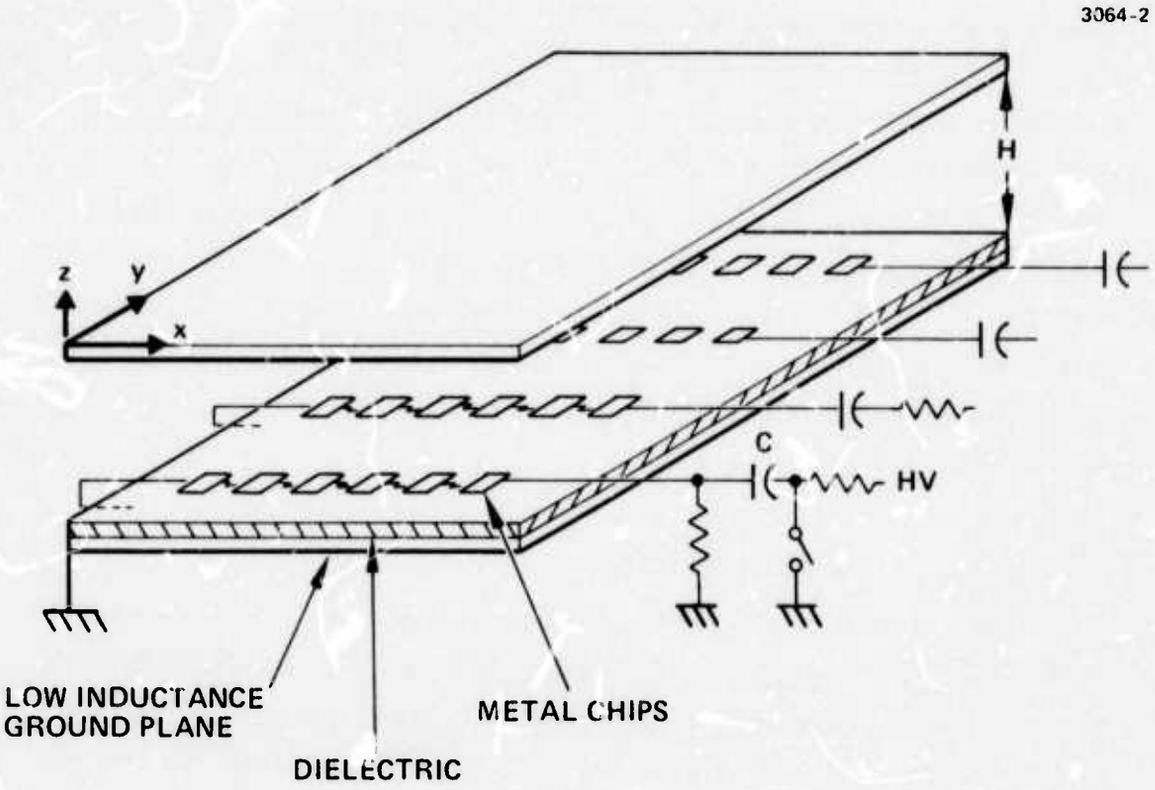

Fig. 6. Cascaded arc discharge system.

This source has been adapted to a 2.5 x 15 x 50 cm^3 discharge device (discussed later) with approximately a 200 J/ℓ-atm input energy obtained. It is of interest to compare this source with individual arcs as used for the results obtained in Section II, and with flashlamps, where estimates can be made from Levine's work at MIT.[4] Such a comparison is made in Table II, where we assume for these calculations that the radiation from each source is sufficient to give photoionization at a level to produce the 200 J/ℓ-atm input discharge energy over a scale length of at least 10 cm. We see that the cascaded arc discharge scheme requires less energy than either flashlamps or individual arcs. The primary reason for this stems from the better impedance match to the input circuit for this configuration.

TABLE II

UV Source Comparison

Type	Energy Delivered to Discharge, %	UV Energy Required to Give 200 J/ℓ Sustainer Input
Individual arcs	10	$0.5 \frac{J}{cm^2}$
Flashlamps (MIT estimates)	50	3.5
Cascaded arc discharge	25	0.3

T1198

We also note that nearly an order of magnitude more energy is required for the flashlamp configuration. This is expected since for this case two-step photoionization is responsible for the production of the dense plasma with a necessarily higher energy requirement to compete with the loss processes that occur out of the intermediate states (see first Semiannual Technical Report).

B. Input Energy, Gain, and Power Extraction

To test the feasibility of the cascaded arc discharge source to uv sustained plasma conditioning, a medium volume test device was constructed from an existing laser test bed. This device had a Bruce profiled cathode located 2.5 cm from a flat mesh anode. The cascaded arc discharge board was located 2 cm below the mesh anode. Brewster angle windows were employed for use with external laser optics which consisted of a 4.5 m total reflector and a 20% transmitting dielectric coated output mirror.

With this device, considerable input energy, small signal gain, and power extraction measurements have been made. Figure 7 gives typical current traces for the cascaded arc circuit and the sustainer plasma discharge obtained in a uv sustained mode. Figure 7(a) was obtained at an $E/N = 1.7 \times 10^{-16}$ V-cm^2 and Fig. 7(b) at an $E/N = 1.85 \times 10^{-16}$ V-cm^2. For the higher E/N the discharge is terminated by an arc occurring at approximately 22 μs into the pulse. Also, for the arc circuit, ringing occurs indicating that even though this uv source is more efficient there is a certain degree of impedance mismatch because of unavoidable circuit inductance.

The energy input to the discharge was calculated by integrating the area under sustainer current curves such as these and then multiplying by the dc bias voltage. For the results of Fig. 7 this corresponds to about 350 J input which was the maximum value obtained for all cases run. By operation at higher bias voltages arcing occurred much earlier in the pulse and hence led to the attainment of smaller input energies. The calculation of energy density depends on the discharge volume (which at this time has not been determined with a high degree of accuracy). However, taking the physical size of the electrode of 15 cm by 50 cm as the discharge area we find that an input energy density of 200 J/ℓ-atm has been obtained for the above case.

The small signal gain was also measured for various mixtures, bias voltages (E/N), and position. A typical gain waveform is shown in Fig. 8. This trace was obtained at a point of 3.5 mm from the

3064-3

CO_2 N_2 He 0.028 | 0.472 | 0.50
Tri-n-PROPYLAMINE 0.3 Torr
P_{TOTAL} = 700 Torr

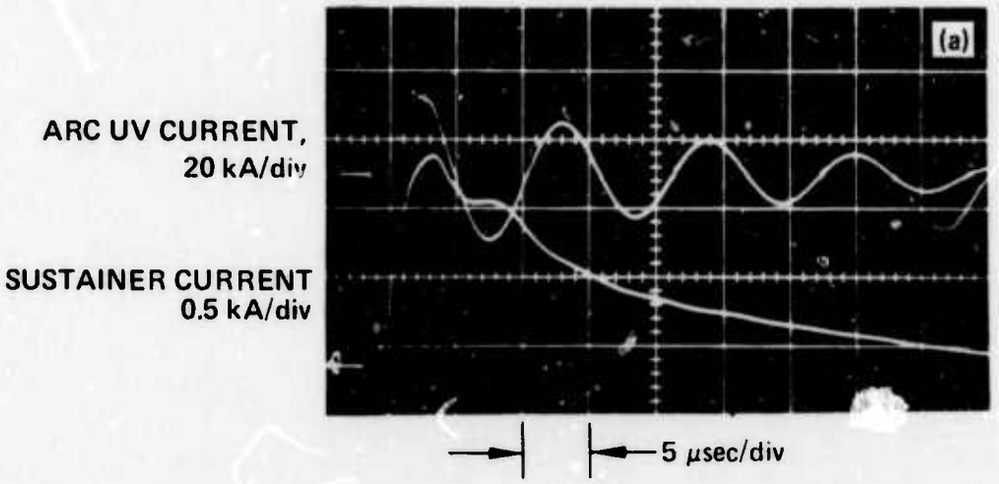

3064-4

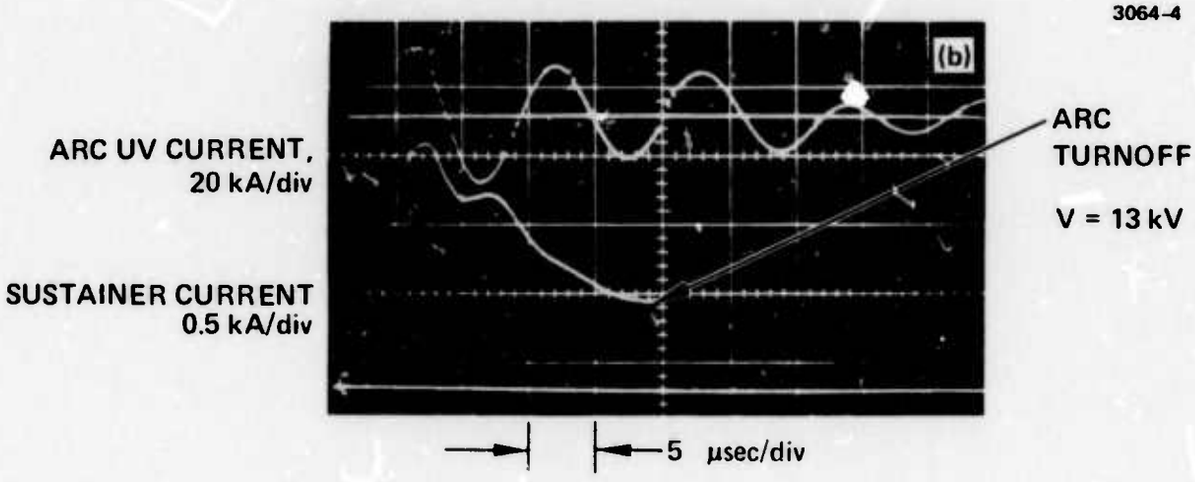

Fig. 7. Sustainer current and cascaded arc discharge current waveforms.

3064-5

CO_2 N_2 He 0.028 | 0.327 | 0.645
Tri-n-PROPYLAMINE 0.3 Torr
P_{TOTAL} = 700 Torr

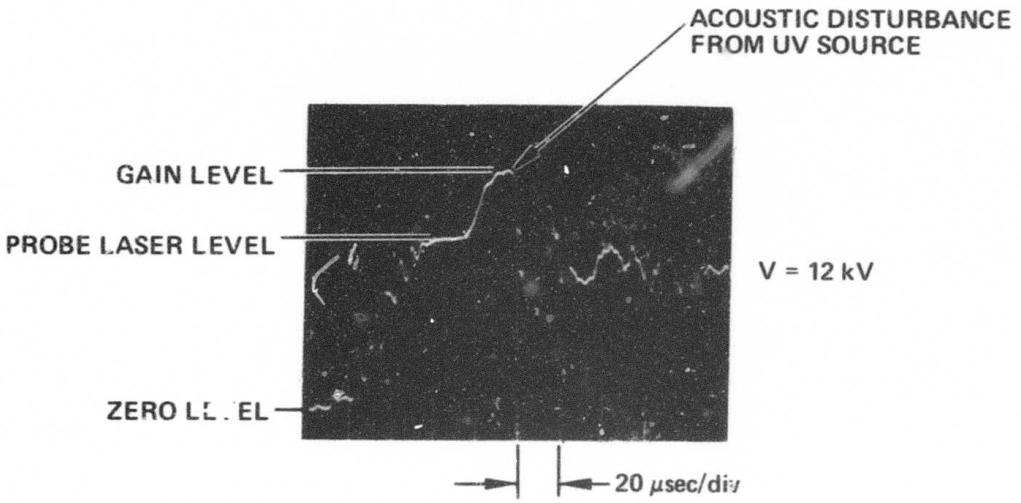

Fig. 8. Small signal gain waveform at position 1.

mesh anode, position 1 (see Fig. 9 for orientation), which corresponds to a location approximately 2.5 cm from the cascaded arc discharge uv source. From this trace the arrival of the acoustic disturbance from the uv source to the point where the probe laser is located is evident. The gain is observed to rise continuously throughout the pulse.

The gain distribution across the gap spacing was measured for various bias voltages. The results for a CO_2, N_2, He 0.028/0.472/0.50, 0.3 Torr tri-n-propylamine mixture are shown in Figs. 10 and 11. In Fig. 10 the gain as a function of bias voltage for the five probe positions is given. The gain varies in a nearly linear manner except for the position nearest the cathode where the gain begins to level off with increased voltage as observed in e-beam pumped systems.[5] In Fig. 11 the gain as a function of position for three bias voltages is given. We see here that the gain increases, as opposed to decreasing, as the distance from the uv source increases. These results are indicative of the field strength increasing to maintain constant current, as n_e decreases moving away from the uv source, and thus rising to a value where possibly some local avalanching by the seed gas is occurring. In addition, the much higher gain near the cathode is a typical result seen for gain behavior in the cathode sheath region.[6] To indicate the very different nature of the gain waveforms near the cathode, the results obtained at position 5 are given in Fig. 12. Figure 12(a) is for 12 kV bias voltage and shows maximum pumping at the beginning of the pulse, because of the much higher n_e levels than obtained at position 1, and subsequent heating of the lower laser level during the remainder of the pulse (see Fig. 8). Figure 12(b) is for 8 kV bias voltage, and thus, much lower n_e levels, and shows pumping throughout the pulse duration but at a rate much lower than the case shown in Fig. 8 which was for 12 kV bias voltage. Another interesting feature of these waveforms is the apparent modulation of the gain, hence n_e by the uv source. This is evidenced by the "ringing" near the start of the gain pulse which has the same period as the uv current ringing. This was observed on all gain traces but was significantly amplified near the cathode.

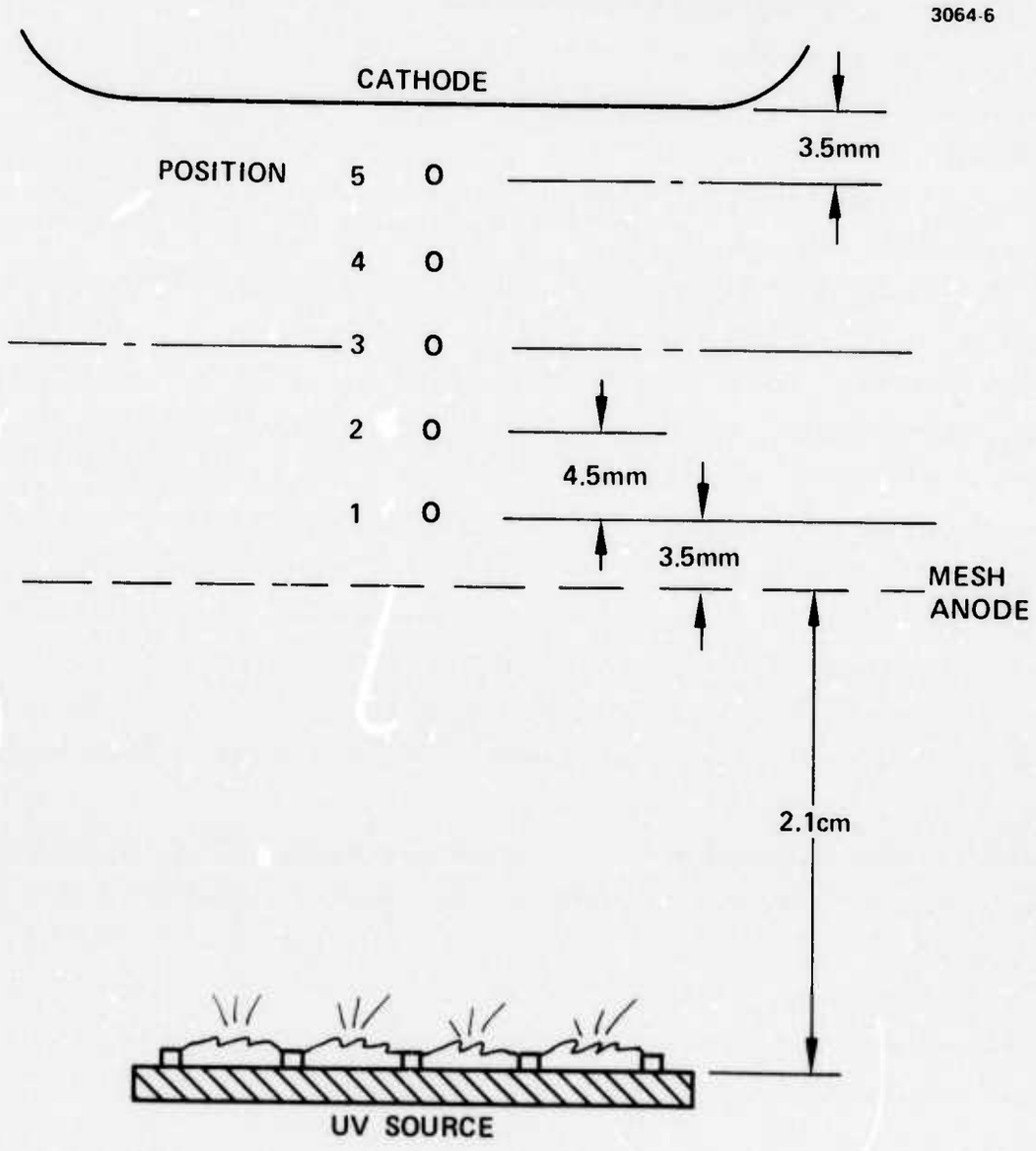

Fig. 9. cw probe laser positions.

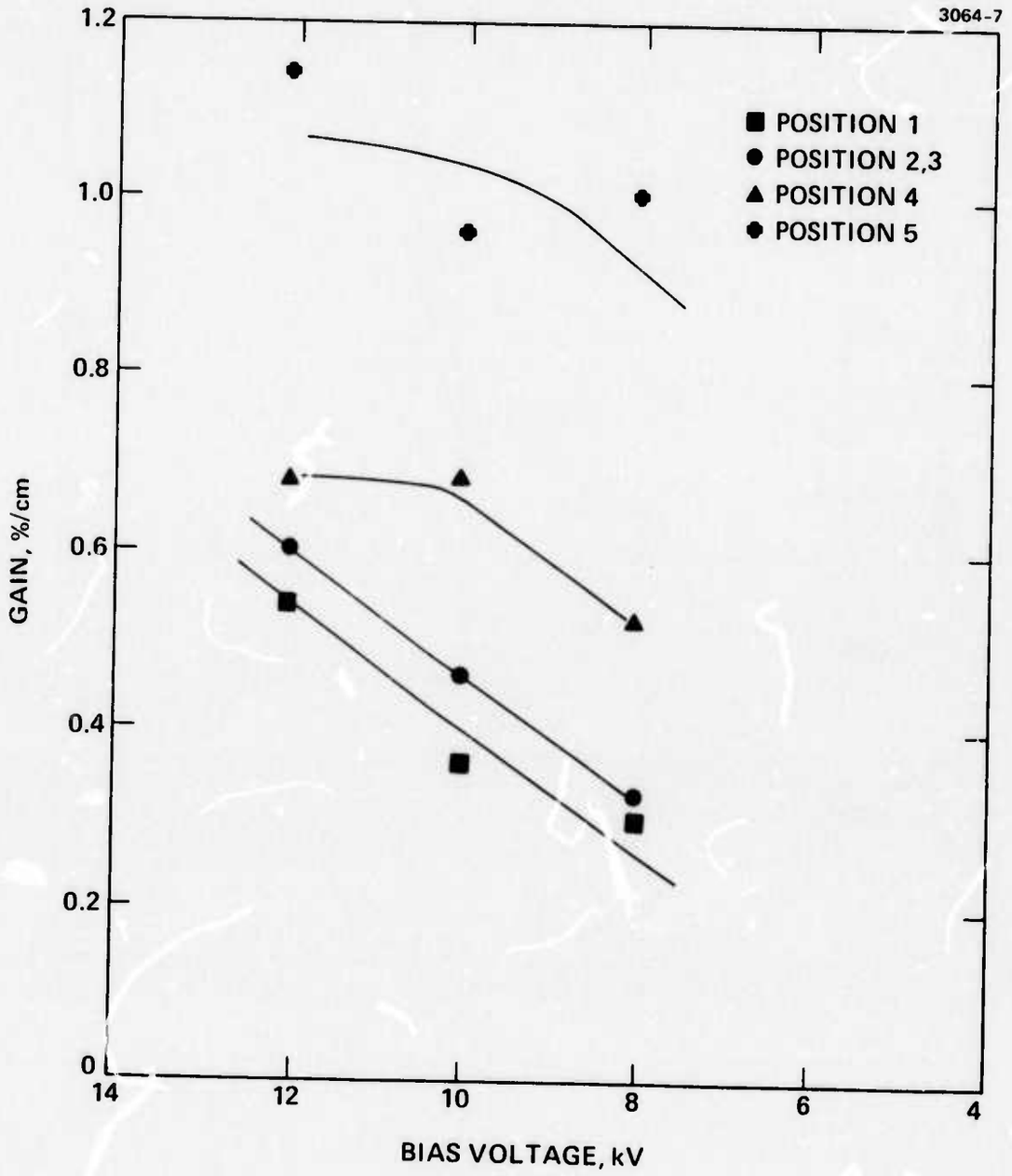

Fig. 10. Small signal gain as a function of bias voltage for 5 positions.

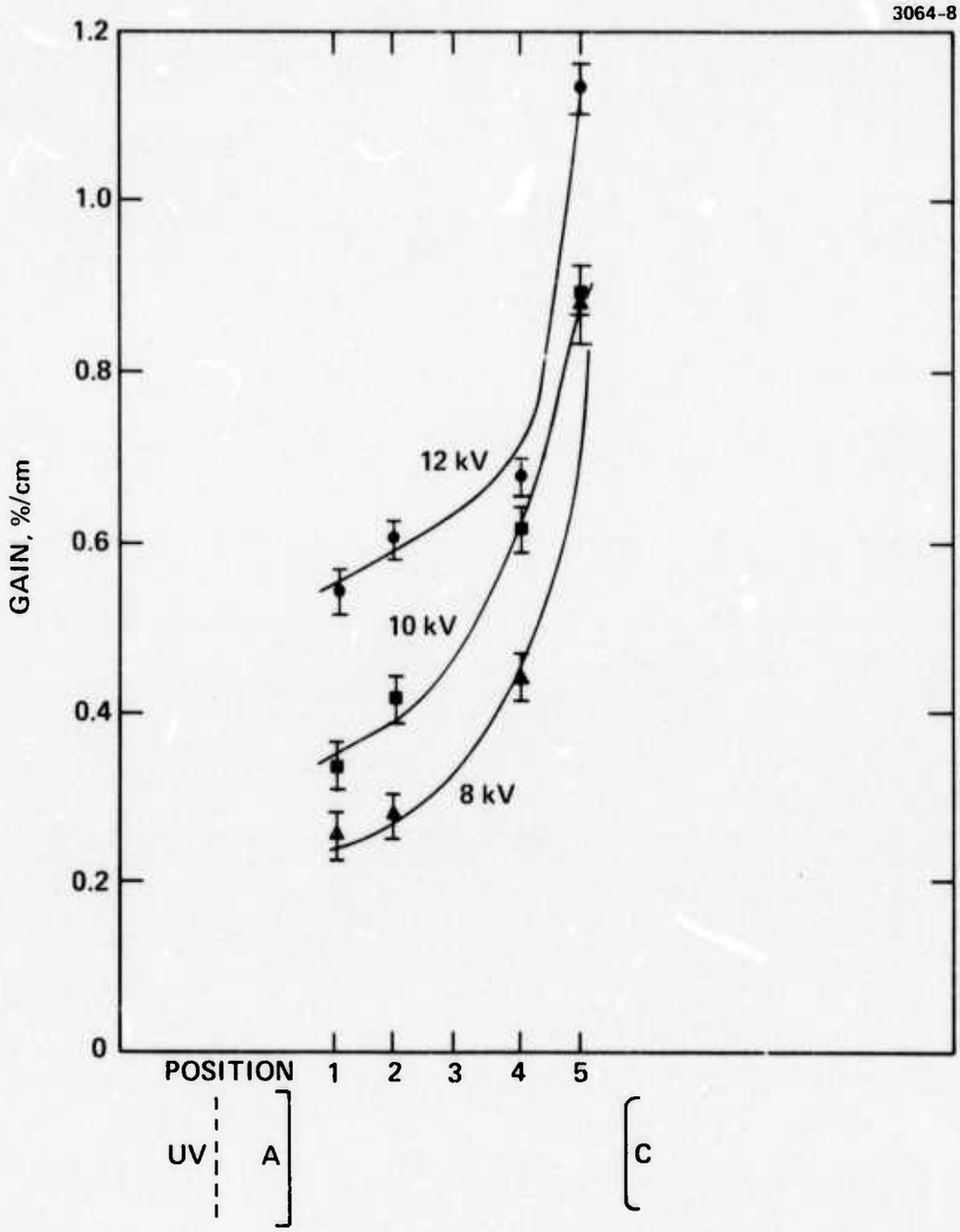

Fig. 11. Small signal gain as a function of position for various bias voltages.

3064-9

CO_2 N_2 He 0.028|0.472|0.50

Tri-n-PROPYLAMINE 0.3 Torr

P_{TOTAL} = 700 Torr

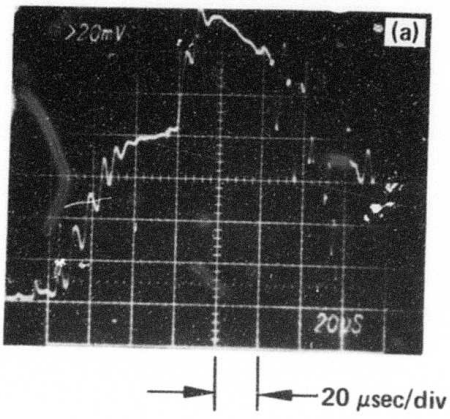

V = 12 kV

20 μsec/div

3064-10

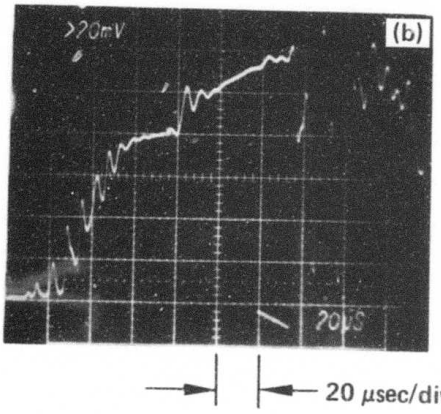

V = 8 kV

20 μsec/div

Fig. 12. Small signal gain at position 5 for two bias voltages.

Further results obtained with lower seed gas concentrations indicated much less of an increase near the cathode as would be expected. Also, experiments were performed by changing the polarity of the electrodes. In this case a much more uniform gain across the gap spacing was obtained but with a reduced magnitude at a value of about 0.6%/cm for the 12 kV bias voltage.

Extensive measurements of laser output were made using a stable cavity arrangement and a Hadron Model 117 calorimeter. The measurements consisted of keeping the uv source energy fixed and varying the bias voltage (E/N) of the discharge and varying the gas mixture. Typical laser pulse shapes are shown in Fig. 13. The laser output shown in Fig. 13(a) and 13(b) corresponds to the cases discussed previously and shown in Fig. 7(a) and 7(b), respectively. Figure 13(a) gives a pulse with a multimode energy of 9.6 J and a pulse length of 37 μs. Figure 13(b) gives a pulse with a multimode energy of 12 J with a pulse that is terminated by an arc which occurs 22 μs into the pulse.

The nearfield burn pattern for the laser output is shown in Fig. 14. This pattern was obtained by using thermal chart recording paper. However, to determine the mode area more accurately, exposed photographic paper was used. This gave a slightly larger area than that shown. With the mode volume established in this manner the laser output energy density can be determined. For the 37 μs pulse of Fig. 13(a), 47 J/ℓ-atm was obtained, and for the shorter pulse (≈29 μs) of Fig. 13(b), 61 J/ℓ-atm was obtained.

To indicate a typical variation in output with E/N, Fig. 15 gives such results for three CO_2N_2He, tri-n-propylamine mixtures. The fact that the output is lower at the largest E/N for the higher CO_2 concentration case results from an arc which occurred early in the pulse and lowered the obtainable input energy.

To calculate the electrical-to-optical conversion efficiency the input energy density is required. Using the estimated 200 J/ℓ-atm value discussed previously we find that an efficiency of about 20 to 25% is obtained.

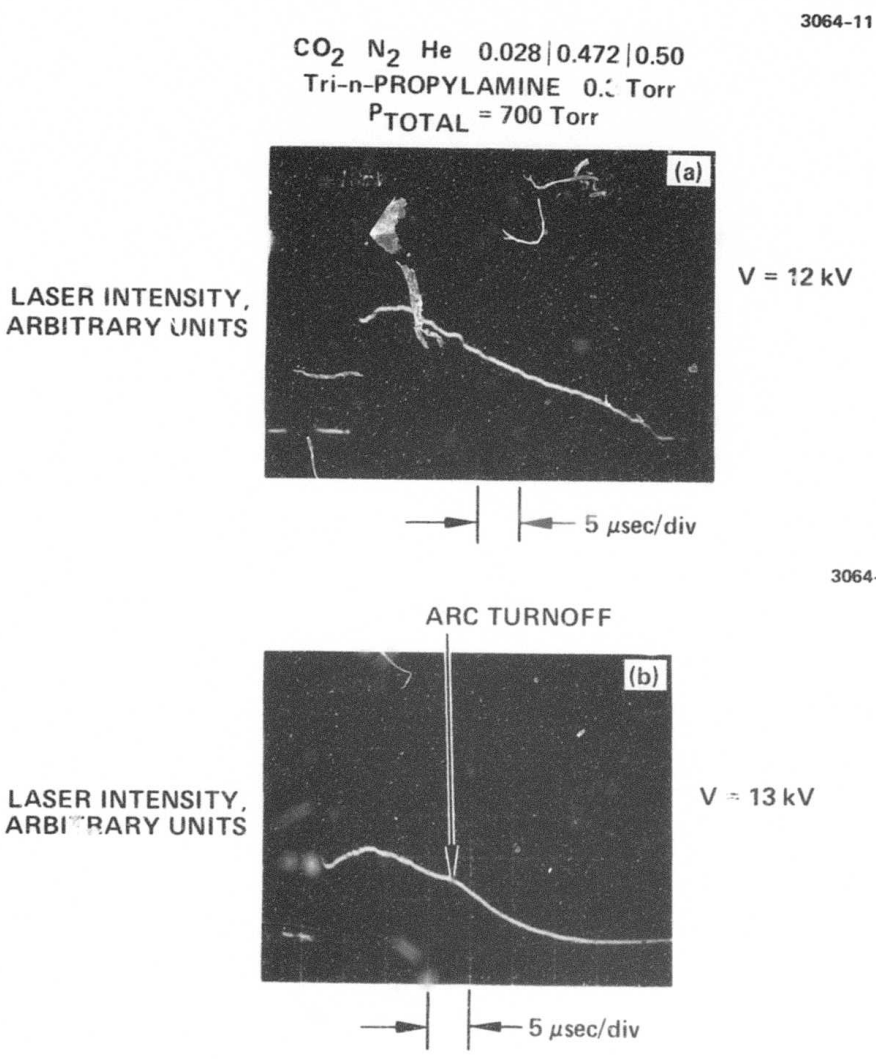

Fig. 13. Laser pulse shape.

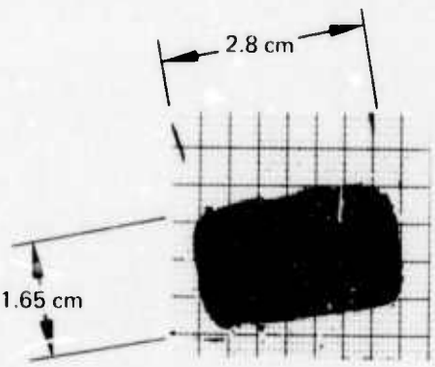

Fig. 14. Near-field burn pattern.

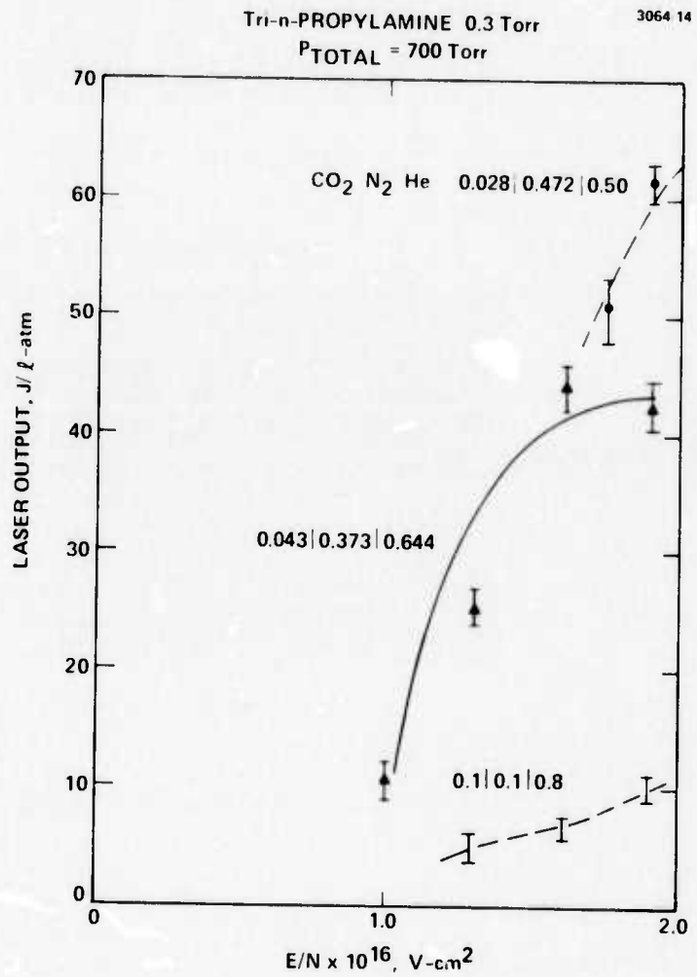

Fig. 15. Laser output as a function of E/N.

Several additional facts that emerged from these laser output measurements were concerned with the effects of the seed gas on system contamination, discharge current, and laser output. After about 1000 firings (which proved the reliability of the cascaded arc circuit board, which showed considerable visible deterioration, but no decrease in obtainable sustainer input energies) no contamination was visible on the salt brewster windows, but a certain degree of residue is apparent on the solid electrode. The laser output decreased with number of shots with typically a 6%/shot falloff observed.

From these results it is apparent that the uv sustained scheme can produce long pulse laser output at sufficient levels to compete with the e-beam sustainer approach. Scalability is the primary remaining problem which will be answered by the work to be carried out in the follow-on contract.

C. UV Photon Flux Calculations

To determine the gain uniformity of a uv sustained discharge, it is necessary to know the electron number density spatial distribution. The electron distribution (n_e) is in turn calculated from the photon flux distribution (I_{uv}) eminating from the uv source configuration. The functional relation between n_e and I_{uv} depends on whether the plasma relaxes via recombination or attachment and whether single step or multistep ionization dominates. For the present experiment, single step ionization and recombination dominates. Thus, $n_e \propto \sqrt{I_{uv}}$ (see Table I of the first Semiannual Technical Report.)

To calculate the flux distribution the following expressions are used (see Fig. 16 for definition of coordinate system). For each arc,

$$B_n(x,y) = \begin{cases} B_n \ \dfrac{\text{watts}}{\text{cm}^2\text{-ster}} & x_n \le X \le x_n + \Delta \\ 0 & y_n \le y \le y_n + a \end{cases}$$

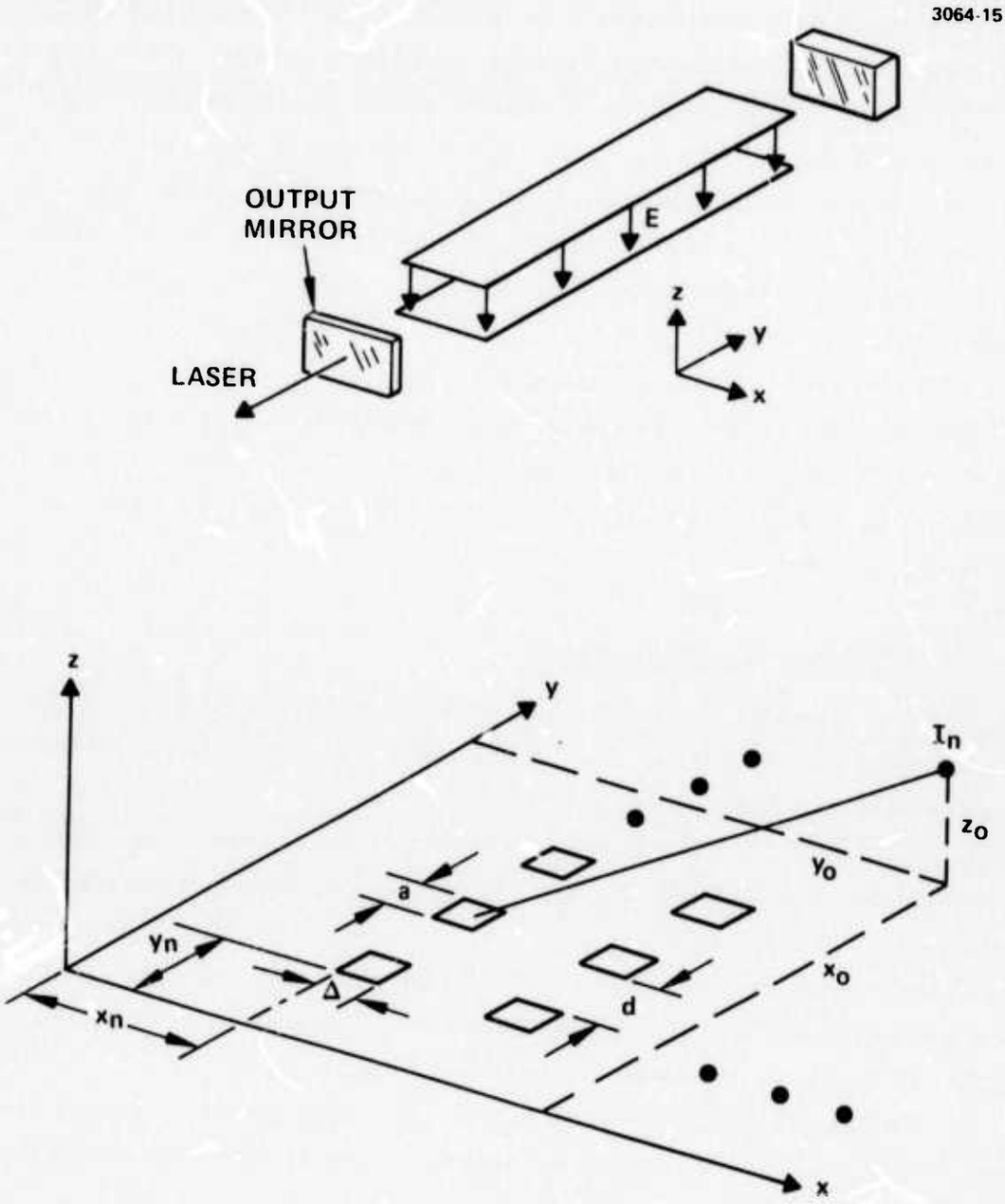

Fig. 16. Photon flux calculation coordinate system.

the intensity is then given by

$$I_n(x_o, y_o, z_o) = \int_{x_n}^{x_n+\Delta} \int_{y_n}^{y_n+a} B_n \frac{z_o}{r^3} e^{-\alpha r} \, dxdy \ ,$$

which can be approximated as

$$I_n \cong B_n \frac{z_o \Delta a}{4} \frac{e^{-\alpha R}}{R^3}$$

where

$$R^2 = \left(x_n + \frac{\Delta}{2} - x_o\right)^2 + \left(y_n + \frac{a}{2} - y_o\right)^2 + z_o^2 \ .$$

Using this expression the flux, and hence n_e distribution, was calculated for several geometries. One such case is that for the geometry of the proposed 20 x 20 x 100 cm^3 device where uv sources are located symmetrically behind the anode and cathode. The electron distribution along each axis for mean free paths of infinity and 10 cm (typical expected value) is given in Figs. 17, 18, and 19, respectively. We see that the largest variation occurs over the distance between the uv sources with a 40% to 50% variation observed.

However, this density gradient exists parallel to the sustainer electric field. Thus, the induced field in the presence of this density gradient will not be uniform across the interelectrode region. In order to satisfy the sustainer current continuity condition, the electric field will be approximately inversely proportional to the electron density. The field strength will be higher in the region where the electron density is lower. Similarly, the field will be lower in the dense region. A consequence of this effect is that the product of the

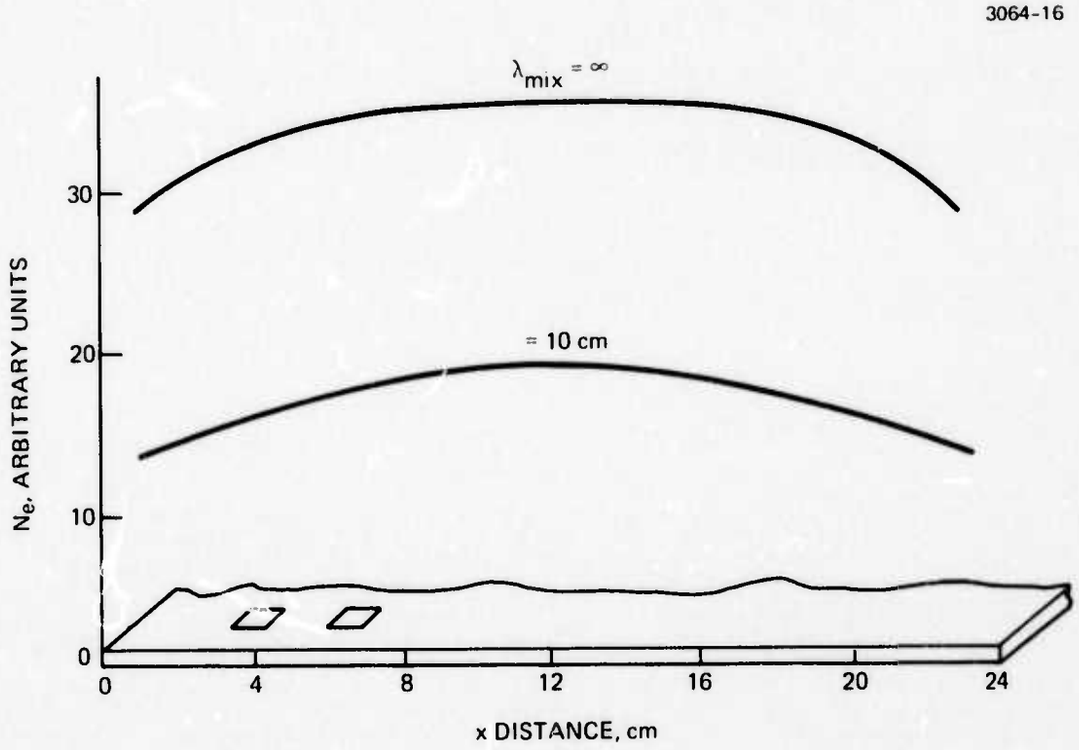

Fig. 17. Calculated electron number density distribution, x direction.

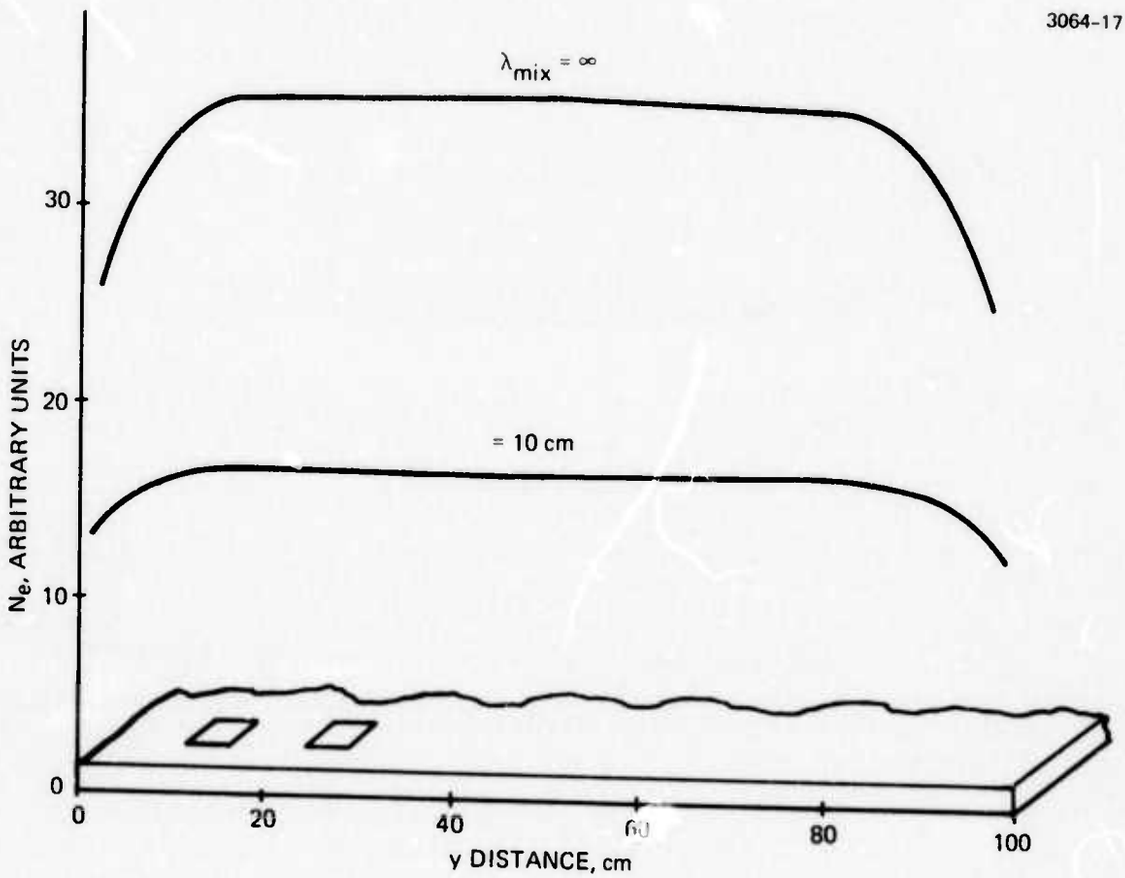

Fig. 18. Calculated electron number density distribution, y direction.

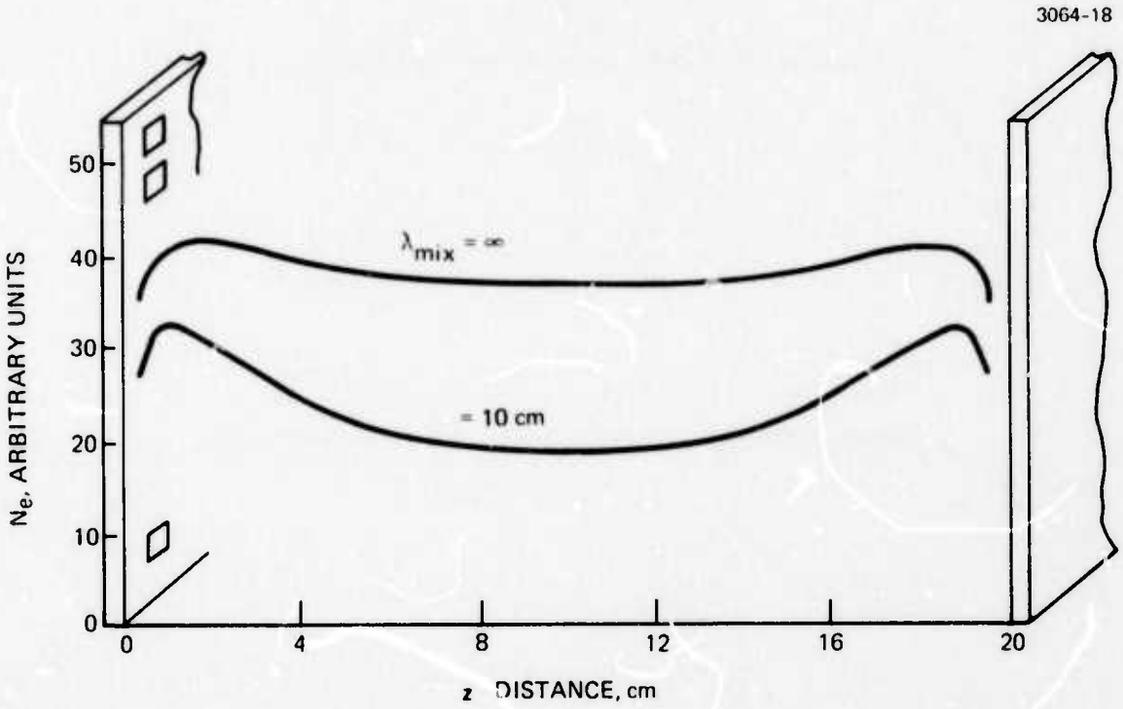

Fig. 19. Calculated electron number density distribution, z direction.

electron density and the electric field will be approximately a constant value throughout the sustainer region. Thus the resulting laser gain distribution will be more uniform in the sustainer region than that of the corresponding density nonuniformity calculated above. Initial measurements of the gain distribution, as shown previously, indicate this trend. This, of course, has strong implications for the gain uniformity that might be expected for the large-scale device studies to be performed during the coming period.

IV. DESIGN STUDIES FOR LARGE-SCALE DEVICE

A program was begun in early November with an ultimate objective of determining the scalability limits of the uv sustained plasma conditioning technique. This is to be accomplished by the design, fabrication, and testing of a large scale (20 x 20 x 100 cm^3) discharge device. This section will review the selected design and present performance estimates for the large-scale configuration.

A. Basic Device Configuration

The general concept of the device is that of a large vacuum chamber in which Bruce contoured transparent electrodes are housed, with uv sources situated behind each electrode. A high energy 50 kJ, 80 kV dc storage bank is used to provide the necessary bias voltage to the electrodes.

The general layout of the equipment is shown in Fig. 20. Figure 21 is an artist's concept of the overall device. Specifically, the vacuum tank is a 4.5 ft diameter by 6 ft long steel tank with 16 feed-through ports for electrical, optical, and gas handling requirements. Figures 22 and 23, respectively, give a cross-sectional and side view of the device. The sustainer electrodes are Bruce contoured to give a 20 x 20 x 100 cm^3 discharge volume. Each electrode has a stainless steel mesh wrapped over its upper surface to allow the uv radiation to pass through. Each electrode is supported on adjustable supports to allow for a variation in gap spacing of from 5 to 20 cm which provides for the necessary scalability limits to be investigated.

The uv source consists of cascaded arc discharge boards with 42 rows of arcs, each row having copper chips 3 mm^2 along the 100 cm discharge length. Each row is energized by a separate 0.1 μF, 25 kV low inductance capacitor. To allow for the capacitors to be located as close to the arcs as possible, and thus reduce the inductance of the circuit, they are placed inside the vacuum enclosure. They are not, however, capable of being subjected to a vacuum environment.

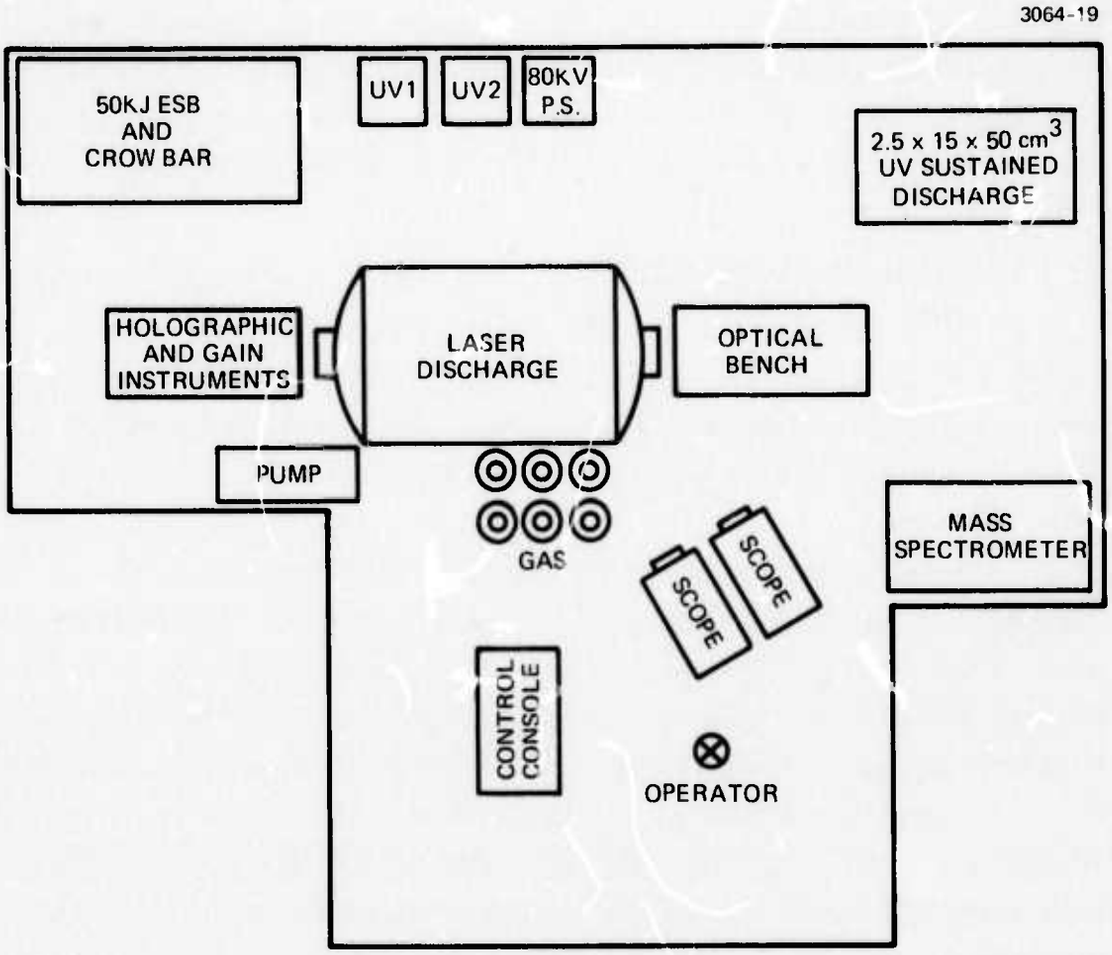

Fig. 20. Equipment layout.

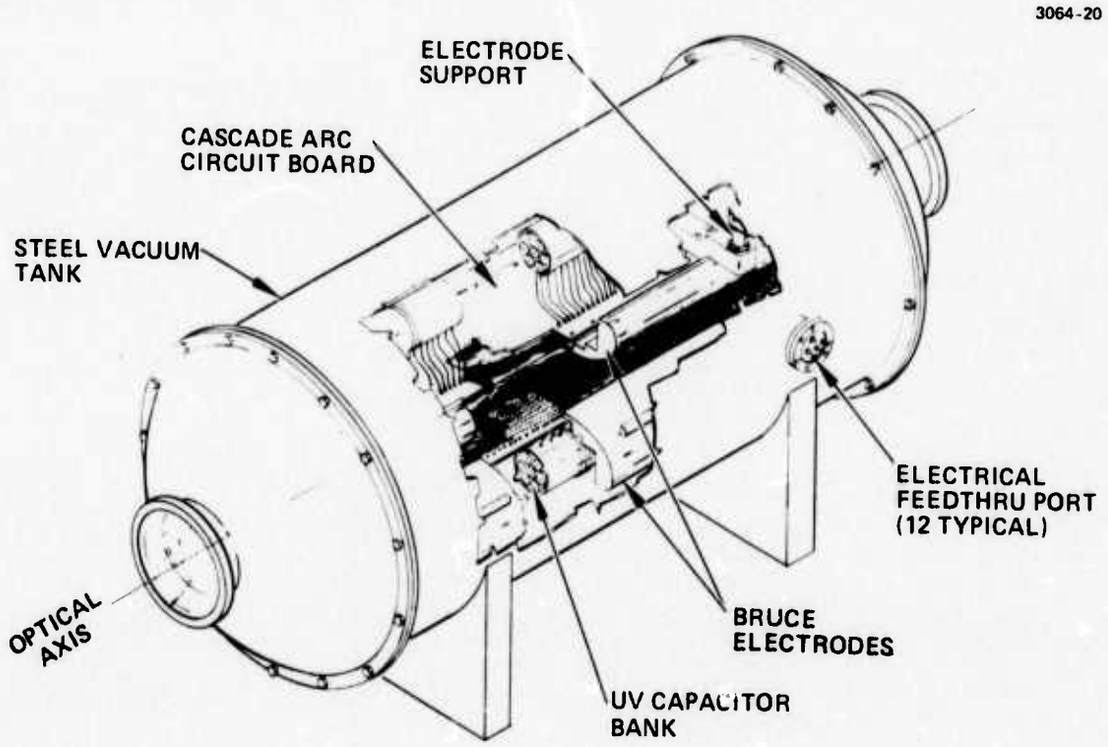

Fig. 21. Discharge enclosure.

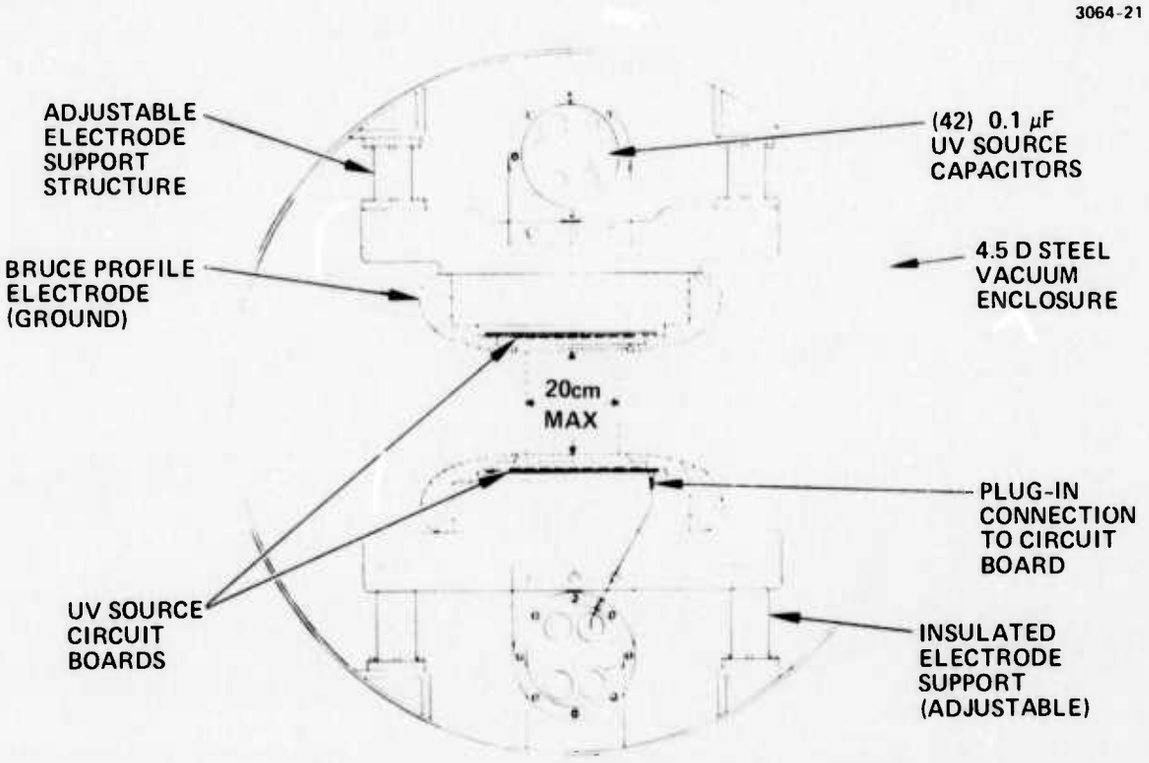

Fig. 22. Device cross section.

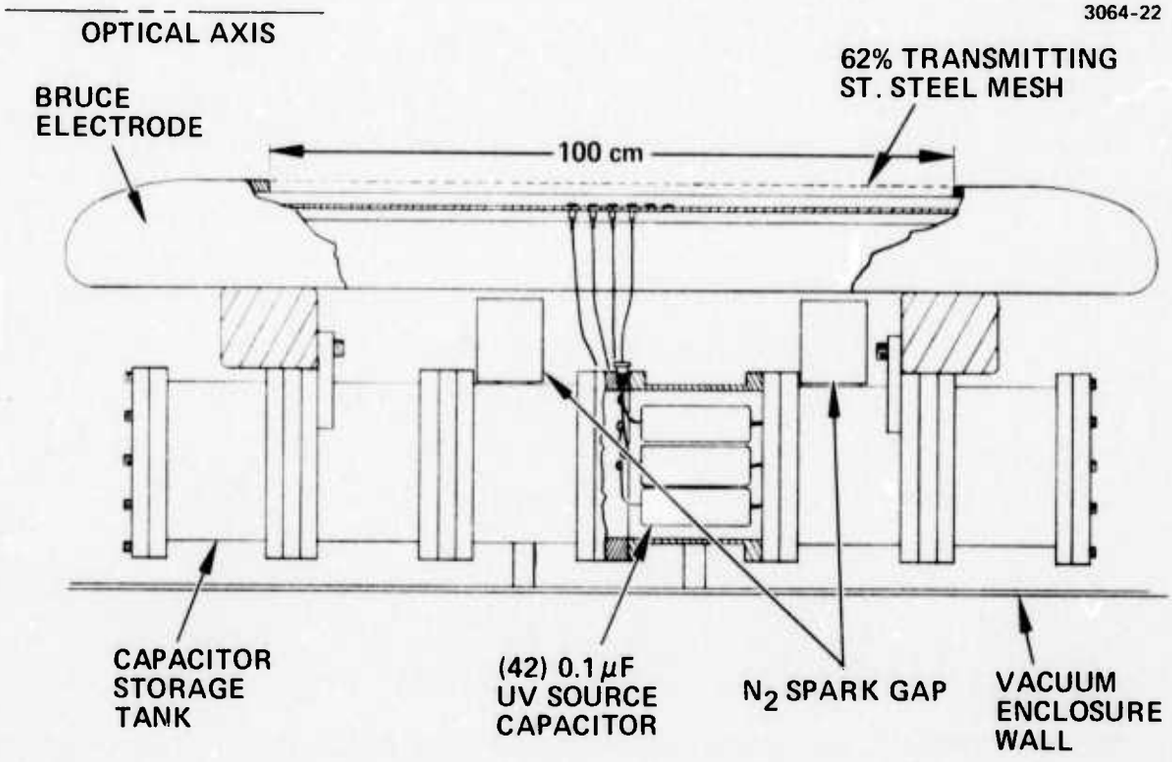

Fig. 23. Device side view.

Therefore, they will be housed in a separate capacitor storage tank built of acrylic tubes as shown in Figs. 22 and 23. Placing them inside the steel tank will also reduce noise signals generated by the high frequency ringing attendant with such uv sources. The N_2 spark gaps which will discharge the uv bank, two for each electrode, are also located inside the tank as shown.

The laser gases, CO_2, N_2, and He will be inserted into the tank through spray bars located on each side of the tank to ensure proper mixing. The seed gas will be added to the system by injection from a calibrated hypodermic syringe.

B. Electrical Characteristics

The short-term power requirements for the uv sustained laser are relatively large, and this energy is more easily stored in capacitors for delivery upon demand. The following is a brief description of the characteristics and major features of the electrical system being fabricated to perform this function.

A schematic of the laser chamber, showing in cross section the discharge electrodes, is presented in Fig. 24. Immediately in back of each electrode are indicated circular arrays of 0.1 μF, 25 kV energy storage capacitors which deliver energy to the arrays of spark gaps. These are interior to the large chamber. Energy to the main electrodes is delivered from an external storage bank through the chamber wall by means of feedthroughs which are also shown in Fig. 24. A single triaxial cable from the external energy storage bank (ESB) is used. The center conductor is at the highest potential (to -70 kV) and is carried through to the lower main discharge electrode. The cable has two outer shields separated by 0.080 in. of PVC. The innermost of these shields, which is at ground potential, is carried through the chamber wall to the upper discharge electrode and conducts the return current from the discharge back to the ESB. The outermost shield is at instrumentation ground and serves to minimize

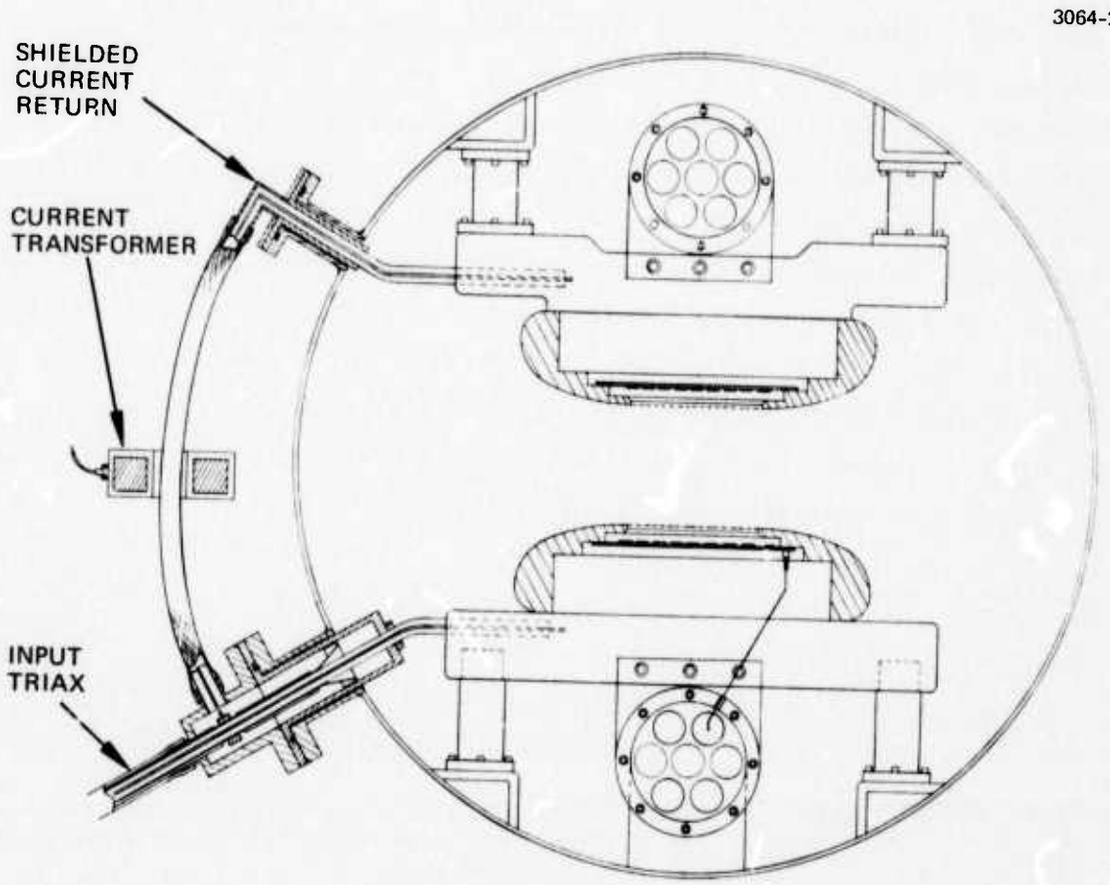

Fig. 24. Electrical feedthrough design.

unwanted pickup in the data retrieval instrumentation. A current transformer surrounds the shielded return cable to measure the discharge current.

Figure 25 shows a more detailed layout of the electrical system. The main ESB consists of 64 capacitors, each rated at 1 μF, 40 kV, charged through a resistor from a high voltage supply. A diverter (crowbar) circuit is provided to dump the bank energy either on demand or upon a system malfunction such as an arc. The diverter consists of a triggerable spark gap in series with two paralleled 4 Ω electrolytic resistors. The ESB and the diverter are packaged in a single oil-filled steel tank and the output is the triaxial cable described previously.

The capacitors in the main ESB can be connected in five basic configurations corresponding to the various discharge configurations. Typical values are tabulated in Table III.

Also shown in Fig. 25 are the two energy storage banks which feed the uv gap arrays. There is a total of 84 capacitors, 42 for each electrode, mounted in arrays of seven. One capacitor is dedicated to each individual row of gaps. Two triggerable spark gaps are used at each electrode, each of which dumps 21 capacitors when fired. The upper electrode uv capacitor bank is isolated to float with the electrode potential. Each electrode system of 42 capacitors is contained in a cylindrical air-filled plastic tube. Throughout the entire electrical system the usual protective devices such as discharge bleed resistors, automatic shorting circuitry, and overvoltage protection are utilized.

Typical operation of the system is indicated by the schematic of Fig. 26. The main ESB and the uv storage banks are charged manually at the control panel. This means of operation will be converted to that of automatic constant current. After the charging is completed, the laser test sequence which has been preset is automatically followed upon depressing an initiate signal. At initiation, all 60 Hz power connections are disabled, after which the four uv bank spark gaps are simultaneously fired. The delay between line power

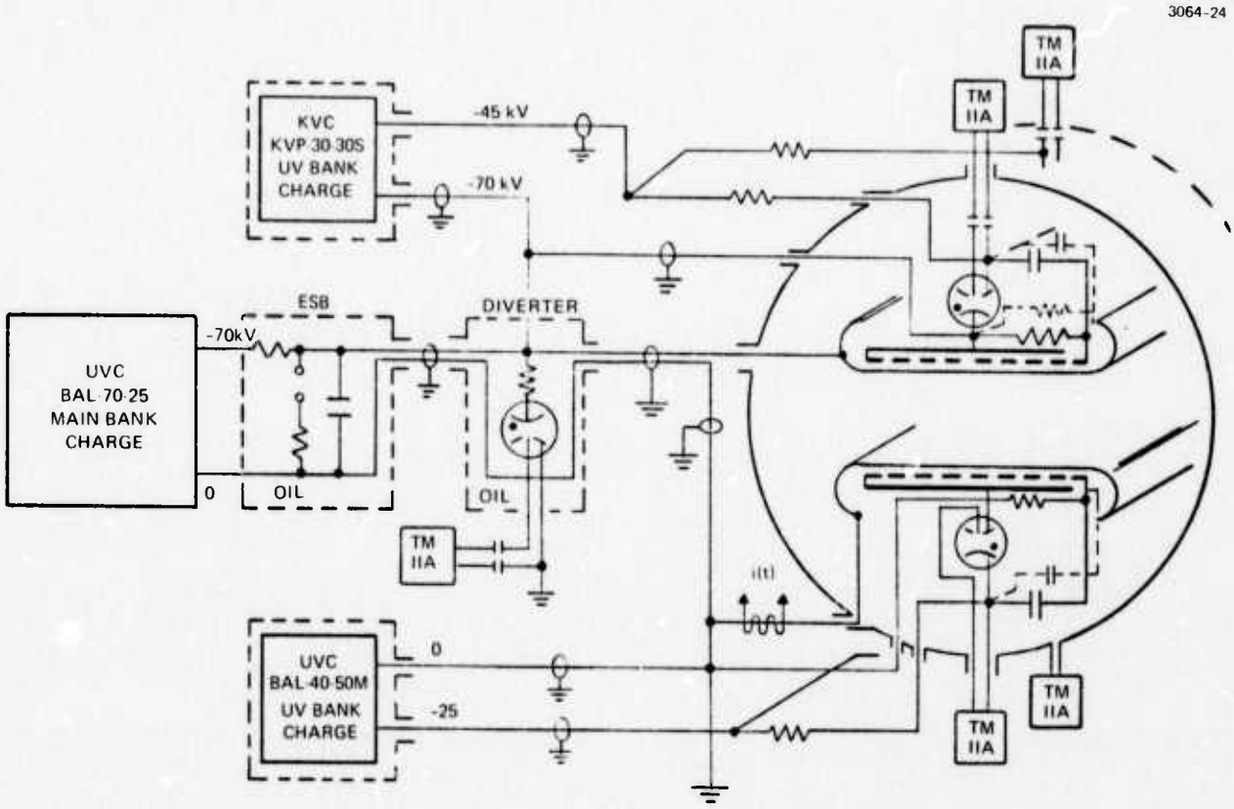

Fig. 25. Electrical layout.

TABLE III

Energy Storage Bank Characteristics

Configuration, μF	Voltage, kV	Maximum Stored Energy, J	Typical Discharge Configuration
A - 8	80	25,600	20 cm gap 10 cm width
B - 16	80	51,200	20 cm gap 20 cm width
C - 64	40	51,200	10 cm gap 20 cm width
D - 32	40	25,600	20 cm gap 20 cm width 0.5 atm
E - 16	40	12,800	10 cm gap 10 cm width

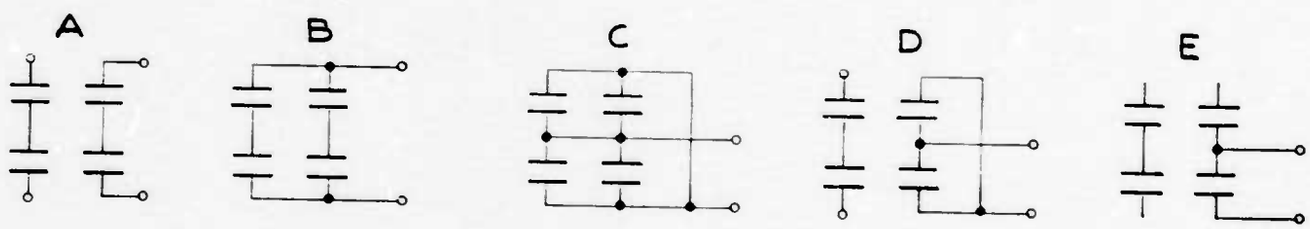

T1196

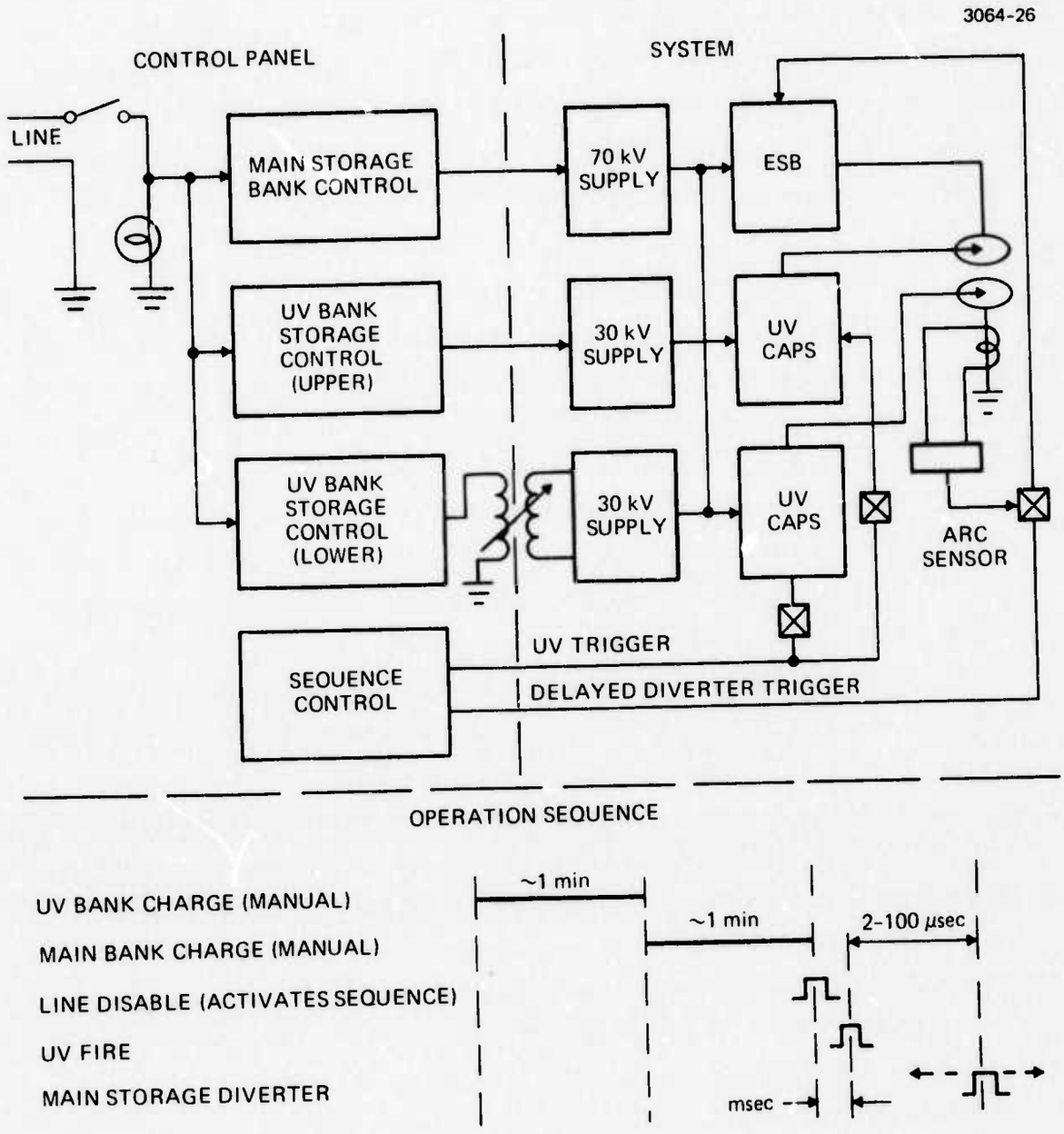

Fig. 26. Operation diagram.

disable and the uv gap firing is on the order of milliseconds. The laser then operates for a preset time period variable between 2 to 100 μs at the end of which the diverter is activated, dumping the remaining charge in the ESB. In the event that an arc is sensed, the 2 to 100 μs delay is overridden and the ESB is automatically crowbarred. There is also a manual override so that the ESB energy may be diverted at any time according to the operator's discretion.

C. Performance Estimates

With the encouraging input energy and power extraction results obtained in the medium volume device described in Section III, we can project possible performance estimates for the large-scale device. These estimates are shown in Table IV.

Three device configurations presented are the medium volume device, discussed previously, and a half- and a full-scale projection for the 20 x 20 x 100 cm^3 device. For these calculations it has been assumed that 200 J/ℓ-atm input energy densities are achievable with a 20% laser conversion efficiency, i.e., 40 J/ℓ-atm output energy. These two figures have, of course, been demonstrated in the medium volume device. The two gap sizes chosen represent the expected operating limits for the device. Based on our projected mixture mean free path of 8 cm (16 cm for symmetrical sources) we feel that a 10 cm gap spacing will be achievable (noting that the uv source is located 2 cm from electrode mesh, because of electrical insulation requirements; thus a 10 cm electrode gap spacing implies 14 cm uv source placement) with the 20 cm spacing providing the capability to determine conclusively the limiting size for a uv sustained plasma conditioning scheme.

TABLE IV

Performance Estimates

Device	2.5 x 15 x 50	10 x 20 x 100	20 x 20 x 100
Input sustainer energy	250 J	4000 J	8000 J
Laser output	50 J	800 J	1600 J
Stored uv	400 J	1450 J	2900 J
Delivered uv	100 J	360 J	720 J
$\frac{\text{UV Stored}}{\text{Sustainer}}$	160%	36%	36%
$\frac{\text{UV Delivered}}{\text{Sustainer}}$	40%	9%	9%
$\frac{\text{Laser Out}}{\text{UV Stored + Sustainer}}$	7.7%	15%	15%
$\frac{\text{Laser Out}}{\text{UV Delivered + Sustainer}}$	14%	18%	18%

T1197

V. SUMMARY AND FUTURE PROGRAM PLAN

A. Summary of Results

Significant results obtained during the last reporting period are listed below.

- Demonstration of a 37 μs laser output pulse with an energy density in excess of 45 J/ℓ-atm in a 1 atm CO_2 laser mixture in a uv sustained mode.
- Characterization of small signal gain magnitude, both temporally and spatially resolved, using a medium volume device (2.5 x 15 x 50 cm^3) with a value of between 0.5 and 1.0%/cm possible.
- Demonstration of a more efficient uv source on the 2.5 x 15 x 50 cm^3 device.
- Calculation of expected electron number density spatial variation for the large-scale device with variations up to only 50% expected.

B. Program Plan for Next Six Months

The program plan to be followed for the remaining six months is shown in Fig. 27. Phase I concerns design and fabrication of the large-scale device. The design as discussed in Section IV is essentially complete at this time. Fabrication will begin when HRL has taken delivery of certain critical items. At the present time, however, because of delivery problems on the large vacuum tank and certain plastics required for the electrode support structure and feedthrough insulation, a one-month delay in initial testing is expected. Referring to the testing program outlined under Task II, this implies that input energy measurements should be made by the end of March. Laser output measurements will be made as soon as sufficient input energy levels are achieved. This represents a minor modification to the program plan as shown, in that gain and medium homogeneity measurements will be made after such laser measurements.

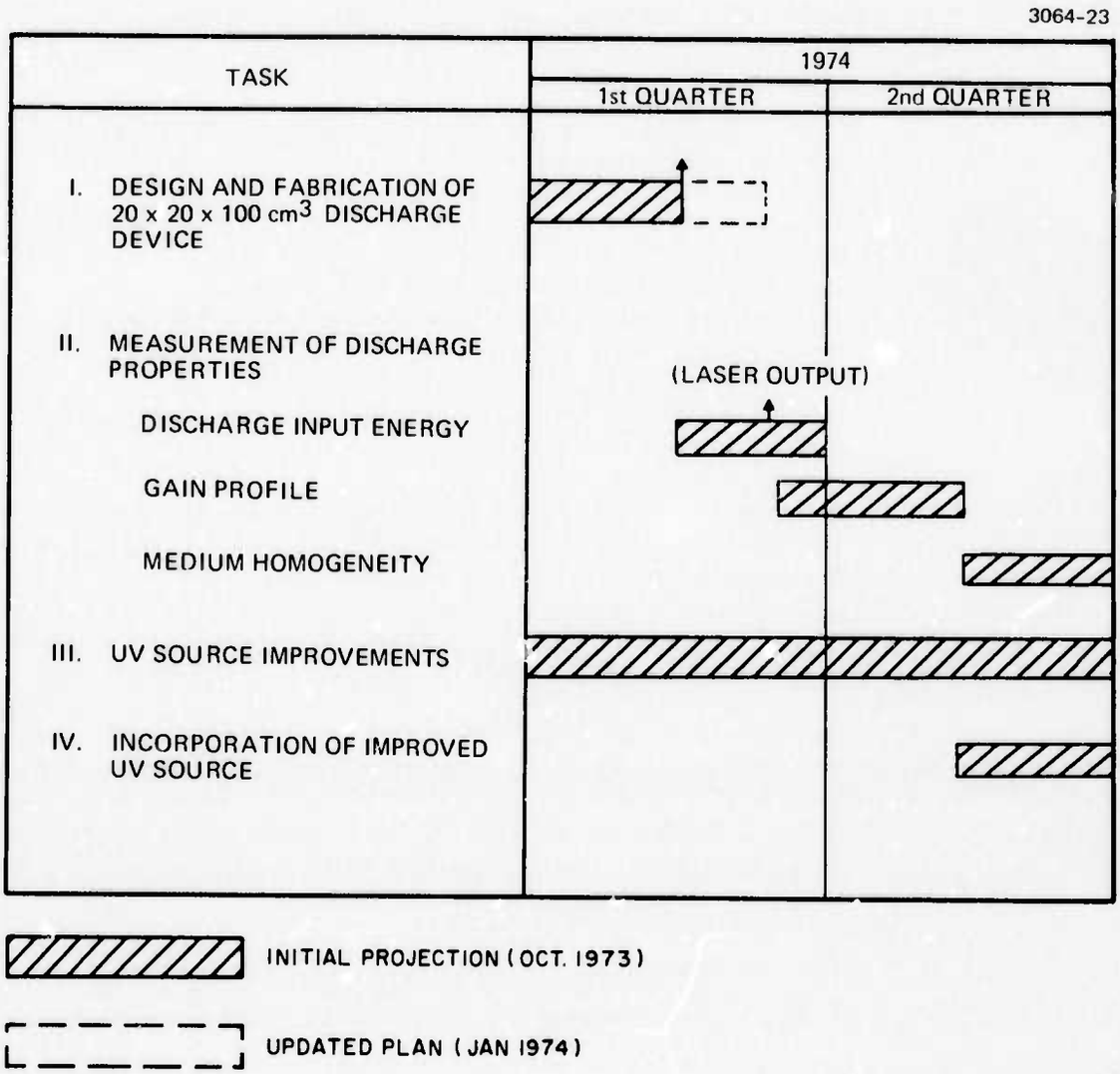

Fig. 27. Program plan.

All components for the gain and medium homogeneity experiments are available at HRL or have been ordered.

Initial laser output measurements will be made using an existing 10 cm diameter stable cavity arrangement, and a 10 x 10 cm^2 aperture calorimeter which has been constructed and used regularly for other high power lasers at HRL.

The effort directed toward improving and implementing new uv sources is to be carried out under Tasks III and IV. Here we are planning a number of tests on improved versions of the cascaded arc discharge scheme. A small experiment for which different metals and dielectrics can be used is being constructed. This will be tested using the McPherson spectrometer to determine the emission wavelengths. In addition, current levels will be investigated together with the long time integrity of such configurations. Expected improvements then will be incorporated into the large-scale device.

REFERENCES

1. R. C. Lind and J. Y. Wada, "Investigation of UV Photo-ionization Sustained Discharge for Gas Lasers," Semiannual Technical Report, Contract N00014-73-C-0287, Hughes Research Laboratories, Malibu, California (1973).

2. F. Frungel, High Speed Pulse Technology (Academic Press, New York, Vol. II, 15-38, 1965).

3. M. C. Richardson, et al., "Large Aperture CO_2 Laser Discharges," IEEE J. Q. E. QE-9, No. 9, 934-939 (1973).

4. J. S. Levine, "Optics Research," Lincoln Laboratory, MIT, issued Oct. 31, 1973.

5. T. F. Stratton, et al., "Electron-Beam-Controlled CO_2 Laser Amplifiers," IEEE, J. Q. E. QE-9, No. 1, 157-163 (1973).

6. T. F. Deutsch and R. I. Rudko, "Spatial and Temporal Dependence of the Gain of a Transversely Excited Pulsed CO_2 Laser," Appl. Phys. Lett. 20, No. 11, 423-425 (1972).